Spectroscopic Investigation of Thulium Doped Tellurite Glasses for 2μm Laser Applications

by

Adil Tolga Görgülü

A Thesis Submitted to the
Graduate School of Engineering
in Partial Fulfillment of the Requirements for
the Degree of

Master of Science
in
Materials Science and Engineering

Koç University

July 2011

Koç University

Graduate School of Sciences and Engineering

This is to certify that I have examined this copy of a master's thesis by

Adil Tolga Görgülü

and have found that it is complete and satisfactory in all respects,
and that any and all revisions required by the final
examining committee have been made.

Committee Members:

_____

Alphan Sennaroğlu, Ph. D. (Advisor)

_____

Mehmet Somer, Ph. D.

_____

Menderes Işkın, Ph. D.

Date: _____

ABSTRACT

In this thesis work, we describe the detailed experiments that were performed in order to investigate the spectroscopic properties of novel tellurite based glass hosts doped with thulium, primarily for 2 μm laser applications. Among the potential candidates as hosts, tellurite glasses (with network former TeO_2) offer several advantages including ease and low cost of production in comparison with crystal counterparts, high chemical stability, and a wide transmission range from ultraviolet to mid infrared (0.35-5.0 μm). Tellurite glasses are known to be moisture resistant, thermally and mechanically stable materials, making them attractive for fiber applications as well. In this study, influence of the doping concentration together with the host composition which affects the strength of cross relaxation and luminescence quantum efficiency was investigated.

In the first part, we worked on thulium doped tellurite glasses with potassium and niobium oxide prepared at different Tm_2O_3 concentrations (Tm_2O_3:(0.70)TeO_2-(0.15)K_2O-(0.15)Nb_2O_5 having Tm_2O_3 concentrations of 0.125, 0.25, 0.5, and 1.0 mol.%) in order to investigate the influence of doping level on the quantum yields and cross relaxation mechanism. The measurements were conducted at different Tm^{3+} ion concentrations for the two emission bands with peaks at 1460 nm ($^3F_4$ level) and 1860 nm ($^3H_4$ level). The Judd-Ofelt theory was used in the analysis of the experimental data. By performing a Judd-Ofelt analysis of the absorption bands, we obtained average radiative lifetimes of 2.57±0.17 ms and 0.35±0.01 ms for the $^3H_4$ and $^3F_4$ levels, respectively. For the $^3H_4$ level, the highest quantum efficiency of 32 % was obtained for the sample doped with 0.125 mol. % Tm_2O_3. The average emission cross section of 6.01×10^{-21} cm^2 measured for the 1860-nm band reveals the potential of this host for the development of 2-μm lasers. Results also show that cross relaxation becomes important as the ion concentration is increased, leading to the quenching of the 1460-nm band and enhancement of the 1860-nm emission.

In the second part, we worked on the tellurite glasses with different glass modifiers in order to investigate the influence of the host composition on the strength of cross relaxation and quantum yields. Two tellurite based glass samples were prepared using niobium-oxide as a glass modifier: (x)Tm_2O_3 : (95)TeO_2 - (5-x) Nb_2O_5 (will be referred as TeNbTm-x) where x=1 and 0.25 mol.% and four samples were prepared using zinc-oxide as a glass modifier: (x)Tm_2O_3 : (80)TeO_2 – (20-x) ZnO (will be referred as TeZnTm-x), where x=1,0.5,0.25 and 0.125 mol.%. We obtained average radiative lifetimes of 2.55±0.07 ms for the TeZnTm samples and 2.76±0.03 ms for the TeNbKTm samples for the $^3H_4$ level. Highest quantum efficiency was obtained as 32% for the 1860 nm emission band and 89% for the 1460 nm emission band for the sample TeZnTm0125. For the sample TeNbTm025 we reported highest obtained quantum yields as 32% and 76% for the 1860 and 1460 nm emission bands, respectively. For the TeNbTm samples, average stimulated emission cross sections were obtained as $2.62x10^{-21}$ for the 1460 nm band and $5.63x10^{-21}$ cm^2 for the 1860 nm band. For the samples containing zinc as a glass modifier (TeZnTm-x), the average emission cross sections were determined to be $2.78x10^{-21}$ and $6.33x10^{-21}$ cm^2 for the 1460 and 1860 nm bands, respectively. These results compare well with values reported in the literature and for the TeZnTm sample we obtained higher stimulated emission cross sections (as high as 7. $36x10^{-21}$ cm^2) in comparison with the tellurite glass samples which was previously analyzed for the 1860 nm emission band. Results suggest that thulium tellurite glass hosts with high emission cross sections are potentially important candidates for the development of 2-μm lasers in bulk as well as fiber configuration.

ÖZET

Bu tezde, 2µm lazer uygulamaları için yeni geliştirilmiş tulyum katkılı tellürit camlarının spektroskopik karakterizasyonu için yapılan deneyler anlatılmaktadır. Potansiyel lazer kaynakları içinde tellürit camları birçok avantaja sahiptir. Kristal malzemelere göre daha ucuz ve kolay üretilebilmeleri, yüksek kimyasal kararlılığa ve morötesinden orta-kızılaltı bölgesine (0.35-5µm) kadar uzanan geniş bir optik geçirgenliğe (transmission) sahip olmaları bu avantajları arasında sayılabilir. Ayrıca, tellürit camları, nem, ısı gibi dış etkilere karşı dayanıklı ve mekanik olarak sağlam malzemeler olarak bilinirler. Bu özellikleriyle fiber uygulamalarında kullanılmaya elverişlidirler. Bu çalışmada, katkılanan iyon derişiminin ve camların kimyasal bileşiminin çapraz sönüm (cross-relaxation) mekanizması ve lüminesans kuantum verimleri üzerindeki etkisi incelenmiştir.

İlk kısımda, katkılanan iyon miktarının lüminesans kuantum verimi ve çapraz sönüm mekanizması üzerindeki etkisini incelemek için potasyum oksit ve niyobyum oksit içeren tellürit camları ($(Tm_2O_3$:$(0.70)TeO_2$-$(0.15)K_2O$-$(0.15)Nb_2O_5$) farklı Tm_2O_3 derişimlerinde (0.125, 0.25, 0,5 ve 1,0 mol. %) hazırlanmıştır. Tepe noktaları 1460 nm ($^3F_4$ enerji seviyesi) ve 1860 nm'de ($^3H_4$ enerji seviyesi) olan iki bant için ışıma (emission) ölçümleri yapılmıştır. Deneysel verilerin analizinde Judd-Ofelt teorisi kullanılmıştır. Soğurma (absorption) bantları üzerinde yapılan Judd-Ofelt analizi sonucunda $^3H_4$ ve $^3F_4$ seviyeleri için ortalama ışıma ömrü (radiative lifetime) sırasıyla 2.57±0.17 ms ve 0.35±0.01 ms olarak elde edilmiştir. Tm_2O_3 derişimi 0.125 mol.% olan örnekte $^3H_4$ geçişi için en yüksek kuantum verimi %32 olarak elde edilmiştir. 1860 nm bandı için ortalama ışıma kesit alanı (emission cross section) 6.01×10^{-21} cm^2 olarak belirlenmiştir. Sonuçlar, kullanılan cam malzemenin 2µm lazer uygulamalarındaki potansiyelini ortaya koymaktadır. Işıma

ölçümleri sonucunda, tulyum iyonu derişimindeki artışın 1460 nm bandında sönümlenmeye (quenching) ve 1860 nm ışımasında güçlenmeye neden olduğu gösterilmiştir.

İkinci kısımda, camların kimyasal bileşimlerinin kuantum verimleri ve çapraz sönüm mekanizması üzerindeki etkisi incelenmiştir. Niyobyum oksit içeren tellürit camları iki farklı Tm_2O_3 derişiminde $(x)Tm_2O_3 : (95)TeO_2 - (5-x) Nb_2O_5$, x=1 ve 0.25 mol.%. (bundan sonra TeNbTm-x olarak anılacaktır) , çinko oksit içeren tellürit camları dört farklı Tm_2O_3 derişiminde $(x)Tm_2O_3 : (80)TeO_2 – (20-x) ZnO$ (bundan sonra TeZnTm-x olarak anılacaktır), x=1 ,0.5,0.25 ve 0.125 mol.% hazırlanmıştır. 1860 nm bandı için yapılan hesaplamalarda TeZnTm ve TeNbTm cam örneklerinin ortalama ışıma ömürleri (radiative lifetime) sırasıyla 2.55±0.07 ms ve 2.76±0.03 ms olarak elde edilmiştir. $^3H_4$ ve $^3F_4$ bantları için lüminesans kuantum verimleri, TeZnTm0125 örneği için, sırasıyla %32 ve %89, TeNbTm025 örneği için sırasıyla %32 ve %76 olarak hesaplanmıştır. Niyobyum oksit içeren tellürit camları (TeNbTm-x) için yapılan ölçümlerde, ortalama ışıma kesit alanları 1460 nm ve 1860 nm bantları için sırasıyla $2.62x10^{-21}$ ve $5.63x10^{-21}$ cm^2 olarak; çinko oksit içeren tellürit camları (TeZnTm-x) için yapılan ölçüm ve hesaplamaların sonucunda ortalama ışıma kesit alanları 1460 nm ve 1860 nm bantları için sırasıyla $2.78x10^{-21}$ ve $6.33x10^{-21}$ cm^2 olarak bulunmuştur. Bununla beraber, önceden incelediğimiz tellürit cam örnekleriyle kıyaslandığında TeZnTm örneklerinden 1860 nm bandı için daha yüksek (7.36 $x10^{-21}$ cm^2 kadar) değerler elde edilmiştir. Elde edilen bu sonuçlar tulyum katkılı tellürit camlarının, hem kitlesel (bulk), hem de fiber olarak 2μm lazer kaynaklarının geliştirilmesinde kullanılmak üzere önemli bir potansiyeli olduğunu göstermektedir.

ACKNOWLEDGEMENTS

Alphan Sennaroğlu is the one whom I would like to acknowledge most with a great patience and kindness during the years he guided and encouraged me at Koç University. Laser Research Lab members deserve great thanks, especially Hüseyin Çankaya. Lab guru in all respects, acknowledgement Oscars goes to him and I am very grateful for his helping hand during my thesis study. All of the members of LRL I would like to thank: Adnan Kurt, M.Natali Çizmeciyan, Aref Mostafazadeh, Ersen Beyatlı, Solmaz Naghizadeh, Işınsu Baylam, and Devrim Köseoğlu. Hoping for the best for all…

I would like to thank my thesis committee members, Mehmet Somer and Menderes Işkın for their invaluable guidance and advices. So many thanks for their support and motivation. Thank God for the family you gave me: My father Yaşar, my mother Müjde, my sisters Özge and Gözde. Here, I wish you the best of everything. Everything that I have is yours; it is to them I wish to dedicate this thesis. Of course, I didn't forget to thank my super best friends Enes Özel, Hüseyin İkizler, and Işınsu Baylam. No need to praise or flatter them, only thing they need to know is that they are awesome! Enes, my home mate, thank you for everything… My MS studies were financed by the TÜBİTAK (The Scientific and Technological Research Council of Turkey) within the BİDEB 2210 framework.

Samples used in this study were prepared at the University of Verona in the research group of Prof. Marco Bettinelli and Dr. Adolfo Speghini.

Table of Contents

List of Tables

List of Figures

Nomenclature

E_0:	Electric field amplitude
ω:	Angular frequency
t:	Time
k:	Wave number
$\hat{k}$:	Unit vector in the wave propagation direction
H':	Perturbing Hamiltonian
q:	Electron charge
z:	Polarization direction of electric field
H_{ab}' :	Matrix elements of perturbing Hamiltonian
Ψ_a :	Wave function of state 'a'
$\hat{p}$:	Dipole moment operator
V:	Interaction potential
E:	Energy
h:	Planck's constant
$\hbar$:	Reduced Planck's constant
$P_{a\rightarrow b}(t)$:	Time dependent transiton probability
$c_a(t)$:	Eingenfunctions of an observable operator
N_a:	Population of ions in the state 'a'
A:	Spontaneous emission rate (Einstein's A coefficient)
B:	Stimulated emission rate (Einstein's B coefficient)
$\rho(\omega_0)$:	Radiation density of monochromatic incident field
k:	Boltzmann's constant
T:	Temperature (in Kelvins)

c:	Speed of the light in vacuum
ε_0:	Vacuum permittivity
τ:	Radiative lifetime
m:	Magnetic quantum number
l:	Angular momentum quantum number
$\vec{P}$:	Electric diplole operator
$\vec{Q}$:	Electric quadrupole operator
$\vec{M}$:	Magnetic dipole operator
$\vec{r}$:	Displacement vector
$\vec{l}$:	Angular momentum vector
$\vec{s}$:	Spin vector
ν :	Frequency
g:	Degeneracy factor
S:	Line strength
f :	Oscillator strength
A_{tp} :	Odd parameters of crystal field operator
n:	Refractive index of a medium
$\overline{\lambda}$:	Mean wavelength
J :	Total angular momentum quantum number
$Y(t,\lambda)$:	Strength of the overlap integral between mixed parity states
$U^{(t)}$:	Doubly reduced matrix element of the unit tensor operator
Ω_t:	Judd Ofelt intensity parameters
N_o :	Ion concentration

$\bar{\nu}$:	Mean wavenumber
β :	Branching ratio
τ_R :	Radiative lifetime
τ_F :	Fluorescence lifetime
η :	Quantum efficiency
σ_{em} :	Stimulated emission cross section
M^2 :	Beam quality
z_f :	Rayleigh range
w_0 :	Beam spot size

Chapter 1: Introduction

1.1 Motivation

Thulium doped systems draw a great deal of interest for numerous laser applications in the near and mid-IR regions of the spectrum because they provide broad emission bands covering the empty region (1400 -2700 nm) between neodymium and erbium systems. In this respect, transitions originating from $^3F_4$ ($^3F_4 \rightarrow {}^3H_4$ and $^3F_4 \rightarrow {}^3H_5$ transitions corresponding 1.5μm and 2.5μm emissions) and $^3H_4$ ($^3H_4 \rightarrow {}^3H_6$ transition corresponding 1.9μm emission)energy states are worthwhile to study. For this purpose, we choose to employ 800 nm excitation scheme which gives rise to the formation of two broad emission bands centered near 1.9 μm and 1.5 μm. Employing this pumping scheme is further beneficial because there are many available pump sources at these wavelengths and this pumping scheme provides an additional advantage, namely “two-for-one” process which favors the 1.9 μm emission at higher active ion concentrations.

The broad emission band around 1.9 μm can be utilized to build new mid-infrared laser sources suitable for spectroscopic, chemical, and atmospheric sensing applications[1]. In addition, strong water absorption occurs at these wavelengths, making thulium doped gain media very attractive in the development of lasers for biomedical applications such as tissue welding and ablation [2-3].Therefore, investigation of the novel laser materials, especially thulium doped hosts which fluoresce around 2 μm deserves a great deal of attention, considering ever-increasing demand and need for the new laser sources operating in the near and mid-IR regions of the spectrum.

So far, detailed studies have been conducted on germanate, silica and fluoride glass hosts together with the various crystal gain media doped with rare-earths for 2 μm laser applications [4-6]. However, among the potential candidates as hosts, tellurite glasses (with network former TeO_2) offer several advantages including ease and low cost of production in comparison with their crystal counterparts, high chemical stability, and a wide transmission range from ultraviolet to mid infrared (0.35-5.0 μm) [3, 7-8]. Tellurite glasses are known to be moisture resistant, thermally and mechanically stable materials, making them attractive for fiber laser applications as well [9-10].

Tellurium oxide (tellurite) can only form a glass with the help of other materials, namely network modifiers. Since bulk tellurite glass has three different structural units (TeO_4 bipyramid, TeO_3 pyramid, and polyhedron), a wide range of network modifiers can be incorporated into the glass matrix which enables us to engineer host composition of the

tellurite glasses for our particular purposes. In addition, tellurite glasses can accomodate very high ion concentrations which is not the case for the silicates and germanates [11].

Another important feature of the tellurite glasses is that they have relatively low phonon energies (700-750 cm^{-1}) which reduce the effect of non-radiative decay and results in higher luminescence quantum efficiencies. Although fluoride and chalcogenide glasses provide lower phonon energies than tellurites, they are not widely used by the fiber applications due to their weak chemical and thermo-mechanical stabilities. On the other hand silica glasses are preferred due to their thermo-mechanical robustness. However, their high phonon energies result in higher non-radiative decay rates. In this respect, tellurite glasses are good alternatives to silica and fluoride glass hosts in terms of adopting strengths of both materials and avoiding their weaknesses.

Up to date, most of the effort was spent on Nd^{3+} and Er^{3+} doped tellurite glass systems [12-15]and there are only few studies conducted on the Tm^{3+} doped tellurite glasses primarily for the fiber applications [16-19]. Recently, moderate level lasing from the bulk thulium tellurite glasses was reported [20] and modelocked operation was demonstrated [21]. Tm^{3+} doped tellurite glasses have great potential for the development of 2 μm laser sources for bulk as well as fiber applications. Hence, there is a lot of work to be done to explore the tellurite glass family.

1.2 Outline

Chapter 2 begins with the brief discussion on the quantum description of the light matter interactions. In this chapter derivation of the Einstein's A and B coefficients will be discussed by applying the perturbation theory on the interaction potential. Thus, we will discuss absorption, stimulated and spontaneous emission phenomena in a more quantitative way.

Moreover, we will provide a qualitative discussion on the crystal field theory and gain a better understanding of how principles of the group theory and crystal field theory provided useful tools for rare earth spectroscopy. Second part of the Chapter 2 was dedicated to the investigation of the transition intensities of the lanthanide ions in laser crystals. Here, we will discuss the Judd-Ofelt theory which forms the theoretical background of this thesis and is one of the major contributions to the rare earth spectroscopy.

Chapter 3 is devoted to the spectroscopic characterization of the new type of tellurite glass hosts doped with thulium. We will give detailed analysis on the absorption and emission characteristics of the novel tellurite glass host summarized in the experimental, results and discussion parts. Tellurite samples were prepared in the University of Verona at different doping levels because for new glass matrices, it is further important to investigate the influence of the doping concentration since this can also affect the strength of cross relaxation and luminescence quantum efficiency.

Chapter 4 uses the material discussed in the Chapter 3 in order to investigate the spectroscopic properties of the two new tellurite based glass hosts prepared at different ion concentrations. However, the main emphasis of this chapter is not to discuss the same Judd-Ofelt analysis or describe the experimental methods in the fluorescence measurements once again. Rather, we will try to make a comparative analysis on the spectroscopic characteristics (i.e. cross sections and luminescence quantum yields) of the tellurite based hosts with different glass modifiers.

In the last chapter of the thesis, we will begin with the brief literature review of the thulium doped tellurite glass lasers. We then describe the experimental procedure that we follow in order to obtain lasing from the thulium tellurite glass samples.

Chapter 2: Theoretical Background

2.1 Quantum Description of Light-Matter Interactions

Consider an electromagnetic wave which consists of transverse electric and magnetic fields oscillating at the frequency ω,

$$\mathrm{E} = \mathrm{E}_0 \cos(\omega t - kx)\hat{z}, \tag{2.1.1}$$

where t is the time, x is the spatial coordinate, k is the wavenumber, and $\hat{z}$ denotes the direction of the polarization. If the wavelength of the EM wave is long compared to the atomic dimensions, indeed this is the case at optical frequencies, we can neglect spatial variation to obtain

$$\mathrm{E} = \mathrm{E}_0 \cos(\omega t)\hat{z}. \tag{2.1.2}$$

Now, we will consider light-matter interaction as a perturbing Hamiltonian by using

$$\mathrm{H}' = -\mathrm{q}\mathrm{E}_0 \mathrm{z}\cos(\omega t), \tag{2.1.3}$$

where z is the polarization direction of the electric field and q is the electron charge and we assume a stationary nucleus.

For a two level system matrix elements of H_{aa}' and H_{bb}' will be zero because, Ψ_a and Ψ_b will be even or odd, and the resulting $\langle \Psi_a | H' | \Psi_a \rangle$ operation is always odd. Defining the dipole matrix element as $\vec{p}_{ba} = q\langle \psi_b | z | \psi_a \rangle$, we get other elements of the perturbating Hamiltonian with the corresponding interaction potential:

$$H'_{ba} = -\vec{p}_{ba} E_0 \cos(\omega t), \quad V = -\vec{p}_{ba} E_0. \tag{2.1.4}$$

Now, consider that these two levels describe the ground and excited states of a particular atomic transition. Assume, we have an atom in the lower level Ψ_a and we shine polarized monochromatic wave on the atom.

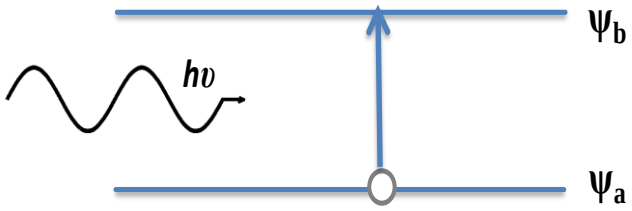

Fig. 2.1.1 Two level system showing absorption

In this case, the atom will interact with light and absorb at the energy corresponding the frequency of $E_b - E_a/\hbar$. Then, the atom will go to the upper level with a certain transition

probability. If we apply time dependent perturbation theory for our specific case (sinusoidal perturbation), we would obtain this transition probability as follows:

$$P_{a\to b}(t) = |c_b(t)|^2 \cong \frac{|V_{ab}|^2}{\hbar}\frac{\sin^2[(\omega_0-\omega)t/2]}{(\omega_0-\omega)^2}. \qquad 2.1.5$$

Here, we choose the initial conditions ($c_a(0)=1$ and $c_b(0)=0$) so that we start from the ground level. This describes the absorption process. If we think that our system is populated in the upper state, ($c_a(0)=0$ and $c_b(0)=1$) we will obtain the same equation with the indices reversed. Einstein predicted this mechanism now known as stimulated emission. This revolutionized the study of optical interactions, giving birth to the concept of LASER.

Yet, there is another important mechanism called spontaneous emission which accounts for the radiative decay. This phenomenon can be explained as follows: Atom in the excited state makes transition to the ground state releasing a photon even in the absence of the perturbative field (zero-point radiation triggered transitions).

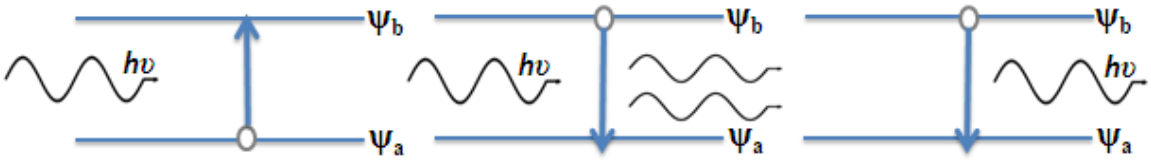

Fig. 2.1.1 Two level system showing absorption, stimulated emission, spontaneous emission

2.1.1 Einstein's A and B Coefficients

Here, we will discuss absorption, stimulated and spontaneous emission phenomena in a more quantitative way. Now, we will again consider a two- level system but this time we have atoms in the ground state (N_a) and in the excited state (N_b) to start with. Let A be the spontaneous emission rate, B_{ba} the stimulated emission rate and B_{ab} the stimulated absorption rate. Now, we can write down the rate equation for the upper level as follows:

$$\frac{dN_b}{dt} = -N_b A - N_b B_{ba}\rho(\omega_0) + N_b B_{ab}\rho(\omega_0) \quad . \qquad 2.1.1.1$$

Here, $\rho(w_0)$ is the radiation density of the monochromatic incident field. In thermal equilibrium $\frac{dN_b}{dt} = 0$ thus radiation density becomes:

$$\rho(w_0) = \frac{A}{\left(\frac{N_a}{N_b}\right)B_{ab} - B_{ba}} \qquad 2.1.1.2$$

And from Boltzmann statistics, we have:

$$\frac{N_a}{N_b} = \frac{e^{-E_a/kT}}{e^{-E_b/kT}} = e^{\hbar\omega_0/kT} \, . \qquad 2.1.1.3$$

We further use Planck's blackbody formula for the energy density

$$\rho(\omega_0) = \frac{\hbar {\omega_0}^3}{\pi^2 c^3 \left(e^{\frac{\hbar\omega_0}{kT}} - 1\right)} \,. \qquad 2.1.1.4$$

Comparing equation 2.1.1.2 with 2.1.1.4, we obtain $B_{ab}=B_{ba}=B$ and relation between Einstein's B and A coefficients $A = \frac{\hbar {\omega_0}^3}{\pi^2 c^3} B$ showing us that emission and absorption rates are not independent of each other.

Here, Einstein's B coefficient was the transition rate of the stimulated emission therefore it becomes:

$$B = \frac{dP}{dt}\frac{1}{\rho(\omega_0)} = \frac{\pi}{3\epsilon_0\hbar^2}\,|\hat{p}|^2 \,. \qquad 2.1.1.5$$

As we mentioned earlier, spontaneous emission was the one that is responsible for the radiative decay. Thus, in the following equation, the relation between Einstein's A coefficient with and lifetime τ is provided:

$$A = \frac{{\omega_0}^3}{3\pi c^3 \hbar \epsilon_0}\,|\hat{p}|^2 = \frac{1}{\tau} \,. \qquad 2.1.1.6$$

Derivation of the Einstein's A and B coefficients completes the discussion on the light-matter interactions. One should appreciate the fact that, understanding the quantum

mechanical derivation of Einstein's A and B coefficients and relating them with the observed optical phenomenon is very important.

2.2 Investigation of Active Ions in a Medium

Conducting spectroscopic investigation on activated laser media primarily aims to determine two features: Stark level manifolds of the active ions and the symmetry properties of wave functions of these levels [22]. Stark level manifolds are produced when the degenerate levels of the ions are split because of the crystal field effects. In general, absorption cross section of a transition would not be same as stimulated emission cross section for the same transition [23].

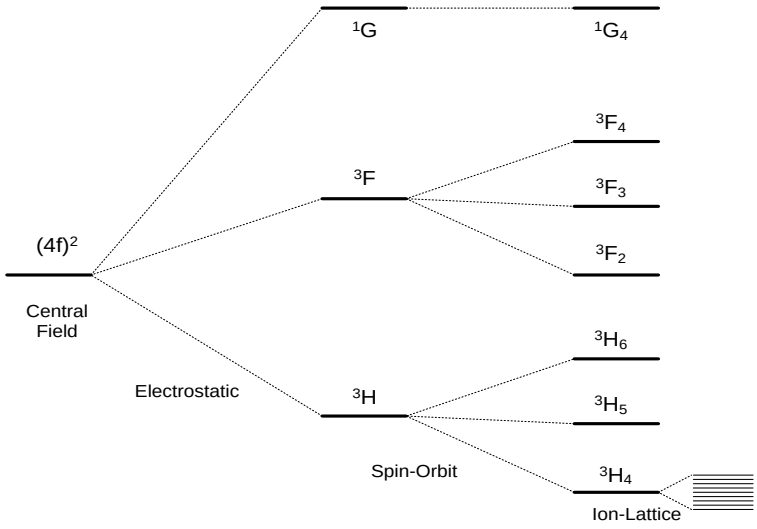

Fig. 2.1.1 Stark level manifolds of the active ions interacting with the crystal lattice

In addition, symmetry properties (i.e crystal field effects, perturbations, etc.) of the wave functions are those that determine selection rules for a particular transition and their strengths. Here, we will make use of crystal field theory and the group theory which provide useful tools to investigate the spectroscopic properties of materials.

First, the effective Hamiltonian of the dopant ion is taken into consideration. This Hamiltonian also includes the interaction between impurity ion and the crystal lattice. Since we have population of electrons (N electrons), the operator which describes the interaction, turns into tensor. In addition to these tensor operators, *crystal field parameters* which are the functions of electron density in the crystal are introduced in order to include the effect of the lattice structure.

Nevertheless, in practice, quantum mechanical calculations of crystal field parameters are tedious and may result in big uncertainties for specific systems [22].Instead, various models have been proposed, in particular for lanthanides, to overcome these difficulties.

A widely used one is the superposition model based on pairwise interactions. As such, wave functions of the localized d and f orbital electrons of the active ions overlap predominantly with the wave functions of the valence electrons of the nearest neighbor ligands. The coordinates of these ligands are the predominant factors that determine the crystal field parameters and the degree of Stark splitting [24].

More generally, the quantity of the Stark levels in these fields can be deduced from S, L, J quantum numbers and can further be realized using the tools of the group theory. Once the point symmetry center of the active ions is known, it is possible to infer about its optical spectra [22]. Nevertheless, this is not the whole story. Although crystal field theory constitutes the basis in understanding spectroscopic properties of media, it would be rather optimistic to expect satisfactory description from the theory for any generic situation. Problems arise especially when we are dealing with the multicenter systems as in our case and further consideration is necessary.

G.Racah made great contributions to the rare earth spectroscopy in 1946, applying group theory to the systems with complex spectra [25]. His pioneering work initiated great developments in the field and peaked with the Judd-Ofelt theory [26-30].

2.3 The Judd Ofelt Approximation to Electric Dipole Transitions

This chapter is dedicated to the investigation of the transition intensities of the lanthanide ions in laser crystals. In the previous chapter, we did a qualitative discussion on the crystal field theory and gained a better understanding of how principles of the group theory and crystal field theory provide useful tools for rare earth spectroscopy. Here, we

will discuss the Judd-Ofelt theory which forms the theoretical background of this thesis and is one of the major contributions to rare earth spectroscopy.

In general, Ln^{+3} ion transitions can be categorized into three: electric dipole, electric quadrupole, and magnetic dipole of which operators are defined as $\vec{P} = \sum_i \vec{r}_i$, $\vec{Q} = -\frac{1}{2} \times \sum_i (\vec{k}.\vec{r}_i) \times \vec{r}_i$, and $\vec{M} = \sum_i \vec{l}_i + 2\vec{s}_i$ respectively. However, in Ref[31], it was shown that electric-dipole and magnetic-dipole transitions are much stronger than electric-quadrupole transitions for lanthanides. It was further shown that for most cases, electric-dipole transitions are the most dominant ones. Therefore, for our specific purpose, we can safely neglect the contributions of magnetic dipole transitions and continue with the investigation of the electric- dipole transitions.

Contribution of electric-dipole transitions to the spontaneous emission probability for a particular transition can be calculated from

$$A(i,j) = \frac{64\pi^4 \nu_{ij}^3}{3hc^3 g_i} \times \sum_{ij} |\langle i|P|j\rangle|^2 \qquad 2.3.1$$

where ν is the wavelength of the transition, g_i accounts for the degeneracy and <i|P|j> are the matrix elements of the electric dipole moments for transitions from state i to j [22].

The sum of the squared matrix elements appearing in the Eq. 2.3.1. is defined as line strength and formulated as follows:

$$S_{ij} = \sum_{ij} |\langle i|P|j\rangle|^2. \quad 2.3.2$$

Following the discussion above, it is obvious that our main objective here is to determine the line (transition) strength of a transition. For this purpose, we will employ absorption methods which provide satisfactory results. Besides, absorption methods offer straightforward solution to spectroscopic characterization of materials in a fairly simple way.

2.3.1 Mixed Parity States

Contribution of electric-dipole transitions to the spontaneous emission probability can be found by following the recipe above. But, electric- dipole transitions between the $4f^N$ states of a lanthanide are quantum mechanically forbidden. However, this restriction can be removed when we put the medium itself into the picture. In this scenario, isolated ions in the crystal will interact with the crystal field potential that can be interpreted as perturbation. As we mentioned earlier in Section 2.2, the Hamiltonian which describes the system of isolated impurity ions will become the "effective Hamiltonian", hence including crystal field –ion interactions.

Suppose that we are trying to obtain the line strength of a particular transition in the form:

$$S_{ij} = \sum_{ij} |\langle \psi_a | P | \psi_b \rangle|^2 , \qquad 2.3.1.1$$

where Ψ_a and Ψ_b are the wave functions of the particular states of interest. As we implied earlier, Ψ_a and Ψ_b will be a linear combination of the ground $4f^N$ configuration $|\phi_{a\,or\,b}\rangle$ with the perturbative crystal field (wave function of the excited state with the opposite parity) denoted as:

$$\langle \psi_a | = \langle \Phi_a | - \sum_e \frac{\langle \Phi_a | V | \psi_e \rangle}{E_a - E_e} \langle \psi_e |$$

$$|\psi_b\rangle = |\Phi_b\rangle - \sum_e \frac{\langle \Phi_b | V | \psi_e \rangle}{E_b - E_e} |\psi_e\rangle . \qquad 2.3.1.2$$

In the equation above, ϕ_a and ϕ_b have the same parity whereas Ψ_e has the opposite parity and V is the perturbative crystal field of which the odd portion is responsible for the mixed parity states. Matrix elements of the electric dipole moments for transitions from state Ψ_a to state Ψ_b can be formulated as follows:

$$\langle \psi_a | P | \psi_b \rangle = - \sum_e \frac{\langle \Phi_a | V | \psi_e \rangle \langle \psi_e | P | \Phi_b \rangle}{E_a - E_e} - \sum_e \frac{\langle \Phi_a | P | \psi_e \rangle \langle \psi_e | V | \Phi_b \rangle}{E_b - E_e} \qquad 2.3.1.3$$

Solving this expression requires to know not only the energies of the excited state and the form of their wavefunctions but also the odd portion of the crystal field potential. Fortunately, Judd and Ofelt came up with the assumptions that greatly simplify the problem. Besides, these assumptions give satisfactory results for many cases except some rare occasions (i.e particularly Eu^{+3} transitions). First assumption states that *excited Ψ_e states are degenerate*. This requires considering an average energy level for the excited state that is $4f^{N-1}$ 5d for the transitions from the ground state $4f^N$. Second assumption is the one which brings great simplifications. It states that "*electron configuration splitting is negligible compared with the energy gap between levels"* [22].

From now on, I will not go into more detailed descriptions on irreducible tensors and matrix operations, since it is beyond the scope of this thesis. I will continue here with a qualitative description and with the key results which help us to reach useful relations for our spectroscopic analysis on thulium doped tellurite systems.

Following the second assumption, E_a-E_e and E_b-E_e becomes constant and equal to each other and energy differences in the denominator can be factored out and the excited state configurations can be treated as they form a complete orthonormal set. In addition, angular parts of the electric dipole operator and crystal field potential can be merged into one representing tensor operator and further reduced by Wigner-Eckart Theorem [32].

For our specific purpose, we will use the approximate solution of the Judd-Ofelt theory for the rare earth ions having $4f^N$ electronic configuration. This will be our ultimate assumption

that will simplify the summations appearing in Equation 2.3.1.3 which is translated into a sum over Stark split J levels and dipole orientations. Assuming equally populated Stark levels and optical isotropy, we finally have an approximate solution of the Judd-Ofelt theory for the oscillator strength:

$$f = \frac{8\pi^2 mc}{3h\bar{\lambda}(2J+1)} n \left(\frac{n^2+2}{3n}\right)^2 \sum_{\lambda=2,4,6} \sum_p \sum_{t=1,3,5} (2\lambda+1) \frac{|A_{tp}|^2}{(2t+1)} Y^2(t,\lambda) \left|\langle \Phi_a | U^{(\lambda)} | \psi_e \rangle\right|^2 \quad 2.3.1.4$$

where A_{tp} are the odd parameters of the crystal field operator, λ and t are even and odd numbers , c is the speed of light in vacuum, *h* is Planck's constant, *n* is the refractive index of the medium, $\bar{\lambda}$ is the mean wavelength of the absorption band, *J* is the total angular momentum quantum number,Y(t,λ) is a constant which reflects the strength of the overlap integral between mixed parity states and inversely proportional to the energy gap of the transition and $U^{(t)}$ is the doubly reduced matrix element of the unit tensor operator. Judd Ofelt intensity parameters are defined as follows:

$$\Omega_\lambda = \sum_p \sum_{t=1,3,5} (2\lambda+1) \frac{|A_{tp}|^2}{(2t+1)} Y^2(t,\lambda) \quad 2.3.1.5$$

With the definition of Judd Ofelt parameters, the Eq. 2.3.1.4 becomes:

$$f = \frac{8\pi^2 mc}{3h\bar{\lambda}(2J+1)} n \left(\frac{n^2+2}{3n}\right)^2 \sum_{\lambda=2,4,6} \Omega_\lambda \left|\left\langle \Phi_a \right|\left| U^{(\lambda)} \right|\left| \psi_e \right\rangle\right|^2. \qquad 2.3.1.6$$

In conclusion, Applying the Judd-Ofelt theory for the rare earth ions having $4f^N$ electronic configuration, the contribution of the electric-dipole transition to the integrated absorption coefficient ,$(\sum_\mu)_{calc}$, for the transitions from the ground state SLJ to an exited state S'L'J' can be obtained by using the equation [28-29].

$$\sum_{\mu} \text{calc} = \frac{8\pi^3 e^2 \bar{\lambda}}{3ch(2J+1)} \times N_o n \left(\frac{n^2+2}{3n}\right)^2 \sum_{t=2,4,6} \Omega_t \left|\langle SLJ|| U^{(\lambda)} ||S'L'J'\rangle\right|^2 \qquad 2.3.1.7$$

In Equation 2.3.1.7, *e* is the charge of the electron, N_o is the Tm^{3+} concentration. Approximate values for Judd-Ofelt intensity parameters appearing in Eq. 2.3.1.7, can be found by using the matrix elements reported in Ref [22] and the experimentally measured integrated absorption coefficient $(\sum_\mu)_{exp}$ which is determined from the absorption spectra of the samples. By using the Judd-Ofelt intensity parameters thus calculated, the spontaneous emission probability *A(J,J')* for a particular transition $SLJ \rightarrow S'L'J'$ can be determined from

$$A(J,J') = \frac{64\pi^4 e^2 \bar{v}^3}{3h(2J+1)} \times n \left(\frac{n^2+2}{3}\right)^2 \sum_{t=2,4,6} \Omega_t \left|\langle SLJ||U^{(\lambda)}||S'L'J'\rangle\right|^2 \qquad 2.3.1.8$$

where $\bar{v}$ is the mean wave number of the transition. Thus the radiative lifetime τ_R for the J[th] excited state is found such that it is equal to the inverse of the total spontaneous emission probability for the transitions originating from that state to all possible J' states : $\tau_R = \frac{1}{\sum A(JJ')}$.

Chapter 3: Spectroscopic Analysis of Thulium Doped Tellurite Glass

3.1 Introduction

Excitation of thulium (Tm)-doped gain media near 800 nm leads to the formation of two unique emission bands around 1460 and 1860 nm spectral regions with numerous important applications.

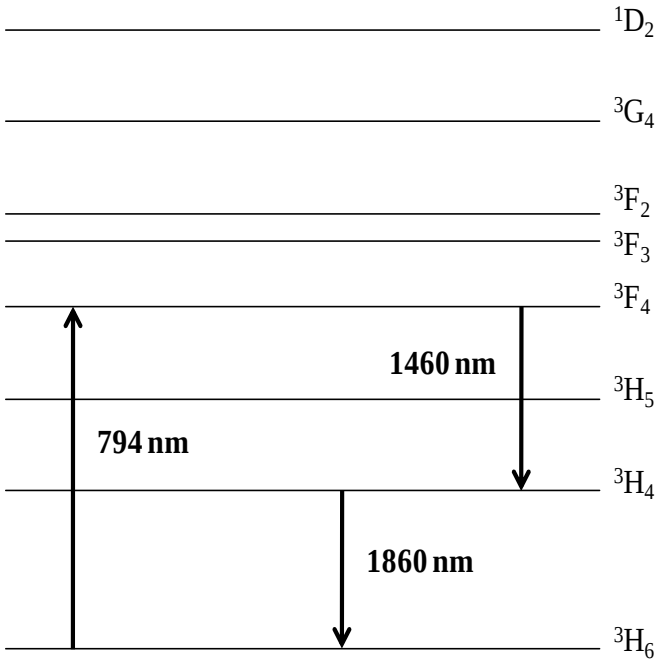

Fig. 2.3.1 Energy level diagram of the Tm^{3+} ions showing the two transitions corresponding 1460 and 1860 nm emission bands with 794 nm pumping scheme.

The broad emission band near 1460 nm is important for the development of optical amplifiers in fiber-optic communication systems [33]. In addition, the broad emission band near 1860 nm can be utilized to build new mid-infrared laser sources suitable for spectroscopic, chemical, and atmospheric sensing applications [1].The broad emission band further enables femtosecond pulse generation from this type of glass hosts in the mid-infrared region [21]. Moreover, strong water absorption occurs at these wavelengths making thulium doped gain media very attractive in the development of lasers for biomedical applications such as tissue welding and ablation [2].

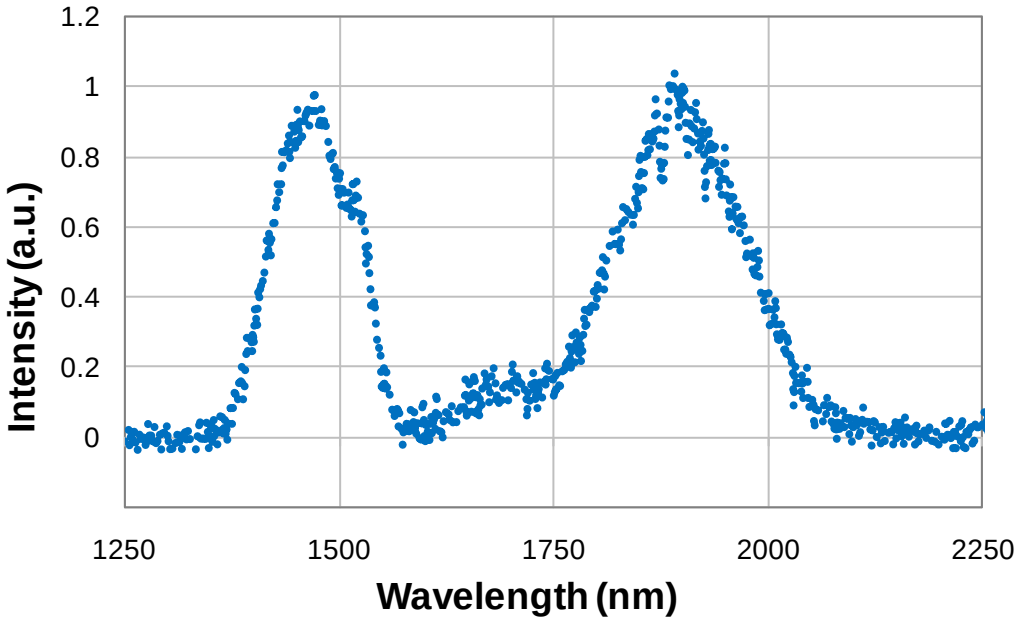

Fig. 2.3.1 Emission bands centered around 1460 and 1860 nm for the 1 mol.% Tm_2O_3 doped tellurite glass sample

In particular, glass hosts can further be utilized as fiber as well as bulk gain media [10].Among the potential candidates as hosts, tellurite glasses offer several advantages including ease and low cost of production in comparison with crystal counterparts, high chemical stability, and a wide transmission range from ultraviolet to mid infrared (0.35-5.0 μm) [3, 7-8]. The relatively low phonon energies (700-750 cm^{-1}) further reduce the effect of non-radiative decay and result in higher luminescence quantum efficiencies. For new glass matrices, it is further important to investigate the influence of the doping concentration since this can also affect the strength of cross relaxation and luminescence quantum efficiency.

We have performed detailed experiments to investigate the spectroscopic properties of a new type of tellurite based host doped with thulium: Tm_2O_3:(0.70)TeO_2-(0.15)K_2O-(0.15)Nb_2O_5 having Tm_2O_3 concentrations of 0.125, 0.25, 0.5, and 1.0 mol. The measurements were conducted at different Tm^{3+} ion concentrations for the two emission bands with peaks at 1460 nm ($^3F_4$ level) and 1860 nm ($^3H_4$ level). The Judd-Ofelt theory was used in the analysis of the experimental data.

3.2 Experimental

Four tellurite glass samples with the composition of Tm_2O_3:(0.70)TeO_2-(0.15)K_2O-(0.15)Nb_2O_5 were prepared from the powders of TeO_2 (99.995 % purity), Nb_2O_5 (99.99 % purity), K_2O (99.99 % purity), and Tm_2O_3 (99.99 % purity). The powder mixtures were melted at 1000 ºC for 15 minutes in a sintered alumina crucible in air and quenched to below the glass transition temperature in a copper mould. The samples were then annealed at 300 ºC for 15 hours. The samples had Tm_2O_3 concentrations of 0.125, 0.25, 0.5, and 1.0 mol. %. The average density of the samples was measured to be 4.47 g/cm^3 by using a picnometer. Samples used in this study were prepared at the University of Verona in the research group of Prof. Marco Bettinelli and Dr. Adolfo Speghini.

The absorption spectra of the samples (see Fig. 3.3.1.1) were measured by using a commercial transmission spectrometer in the range of 400-2000 nm. Background signal due to scattering and surface reflections was subtracted separately for each band for the Judd-Ofelt analysis.

In the emission spectrum measurements, a home-made pulsed tunable Ti:sapphire laser which produced 60-ns pulses at 1 kHz repetition rate was used as the excitation source.

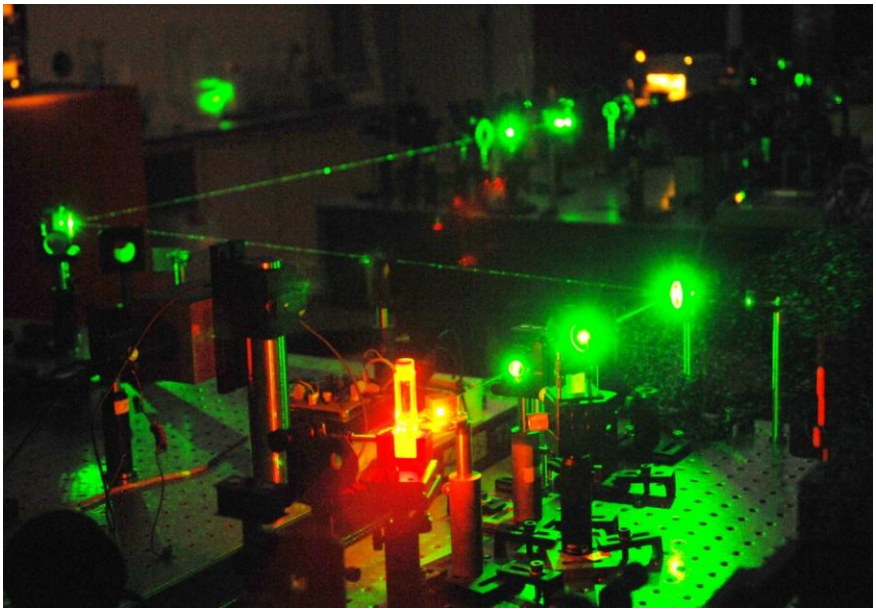

Fig. 2.3.1 Homemade tunable Ti:sapphire laser used as an excitation source in the fluorescence experiments

The wavelength of the laser was set to 794 nm, where the Tm:tellurite glasses have the maximum absorption for this particular absorption band. The emission signal was collected by using a concave gold mirror and imaged into a 0.5 m Czerny–Turner type monochromator (Fig. 3.2.1). The luminescence spectra were recorded with a PbS detector and amplified by a lock-in amplifier in the 1250-2250 nm range. The final spectrum was obtained by taking into account the spectral response of the detector and the gratings of the monochromator.

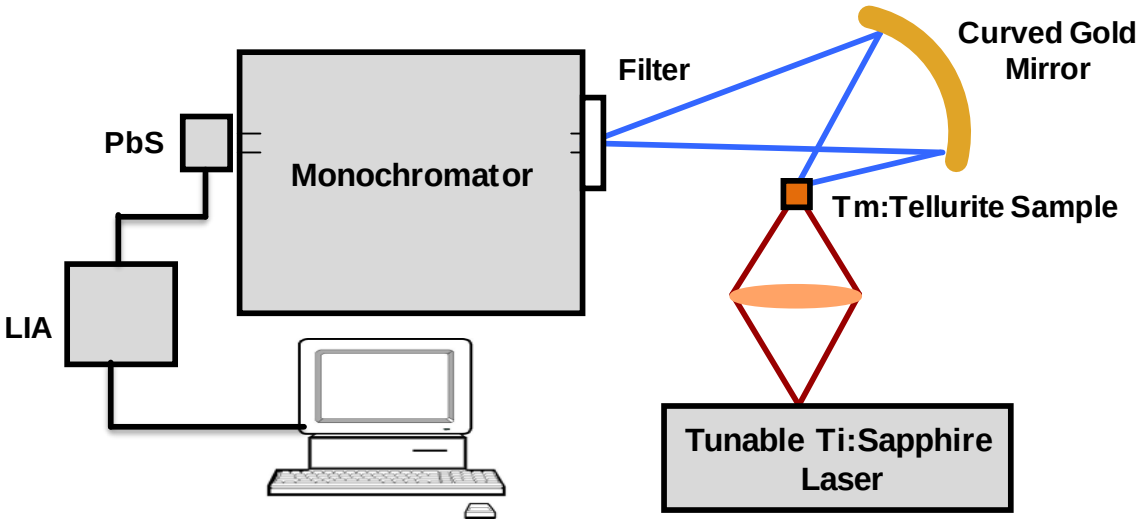

Fig. 2.3.1 Monochromator setup used in emission measurements and lifetime measurements of the $^3F_4$ level (1460 nm band)

In the lifetime measurement of the $^3F_4$ level (1460 nm band), the emission signal at 810 nm corresponding to the transition from $^3F_4$ to $^3H_6$ level was detected by using a monochromator together with a photomultiplier tube. To measure the lifetime of the $^3H_4$ level (1860 nm), the pulse repetition rate of the Ti:sapphire laser was reduced to 100 Hz. The emitted fluorescence around 1860 nm was filtered out by using several band-pass filters and detected with a Ge detector connected to a current amplifier (Fig. 3.2.3).

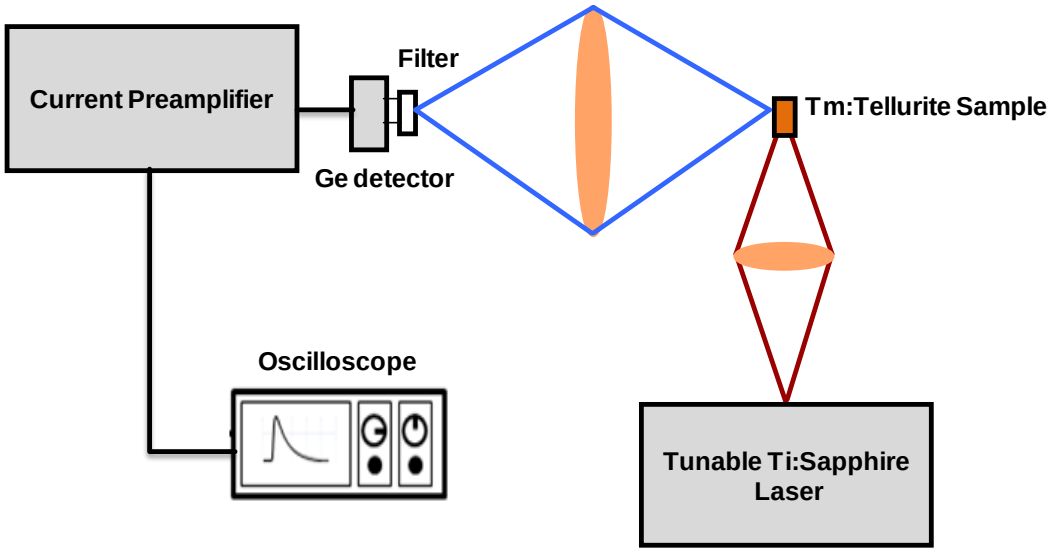

Fig. 2.3.1 Schematic of the setup used in the lifetime measurements of the $^3H_4$ level (1860 nm band)

To determine the fluorescence lifetime for each band of the Tm^{3+} doped glass samples, an exponential curve was fitted to the tail of the measured decaying fluorescence signal. All the measurements were done at room temperature.

3.3 Results and Discussion

3.3.1 Judd-Ofelt Analysis

Judd-Ofelt theory was employed to investigate the dependence of the radiative lifetimes on the Tm^{3+} ion concentration for the $^3F_4$ and $^3H_6$ levels. In the Judd-Ofelt theory of the rare earth ions having $4f^N$ electronic configuration, the contribution of the electric-

dipole transition to the integrated absorption coefficient for the transitions originating from the ground state SLJ to an excited state S'L'J' can be obtained by using the equation [28-29]

$$(\Sigma_\mu)_{calc} = \frac{8\pi^3 e^2}{3ch}\frac{(n^2+2)^2}{9n}\frac{\bar{\lambda}}{(2J+1)}N_o \times \sum_{t=2,4,6}\Omega_t\left|\left\langle SLJ\left\|U^{(t)}\right\|S'L'J'\right\rangle\right|^2 \qquad 3.3.1.1$$

In Eq. (1), e is the charge of the electron, c is the speed of light in vacuum, h is Planck's constant, n is the refractive index of the medium, $\bar{\lambda}$ is the mean wavelength of the absorption band, J is the total angular momentum quantum number, N_o is the Tm^{3+} concentration, Ω_t's are the Judd-Ofelt intensity parameters and $U^{(t)}$ is the doubly reduced matrix element of the unit tensor operator. Approximate values for Judd-Ofelt intensity parameters appearing in Eq. 3.3.1.1 can be found by using the experimentally measured integrated absorption coefficient $(\Sigma_\mu)_{exp}$ and the matrix elements reported in Ref. [22]. The integrated absorption coefficient can also be obtained experimentally for each band by removing the background signal which is due to scattering and surface reflection losses. Figure 3.3.1.1 shows the measured absorption spectra of two glass samples having Tm_2O_3 concentrations of 0.25 and 1 mol. %.

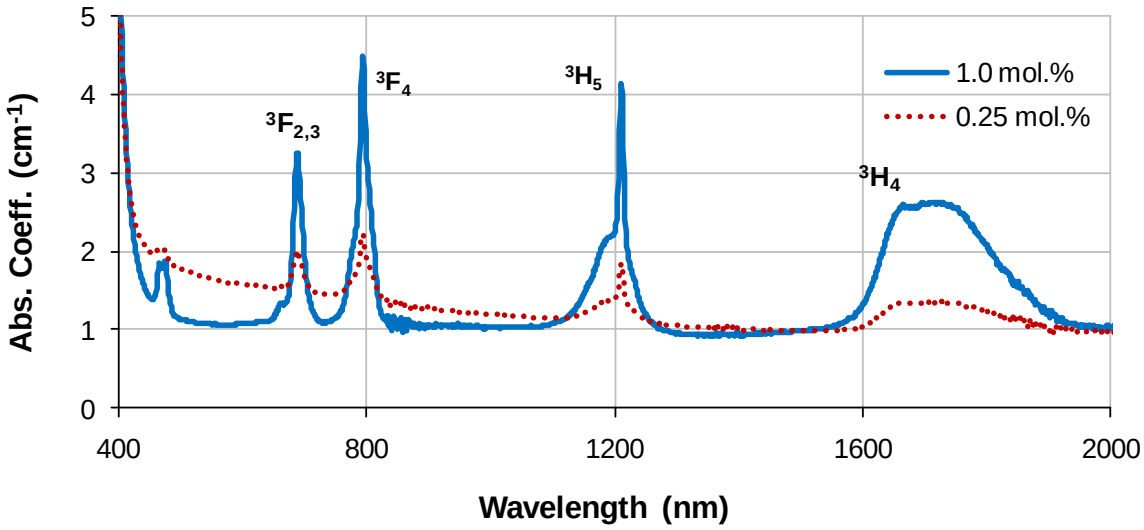

Fig. 3.3.1.1 Absorption spectra of two Tm_2O_3: TeO_2-K_2O-Nb_2O_5 glass samples having Tm_2O_3 concentrations of 1.0 and 0.25 mol. % in the range of 400-2000 nm. The corresponding absorption bands from the ground state ($^3H_6$) are indicated.

In our analysis, we used four ground state absorption bands of Tm^{3+} ion to the $^3F_{2,3}$, $^3F_4$, $^3H_5$, $^3H_4$ levels to determine the intensity parameters as well as the radiative lifetimes. Use of $(\Sigma_\mu)_{exp}$ inside Eq. 3.3.1.1 yields an approximate solution for the system of four equations involving the three Judd-Ofelt intensity parameters. The equation was solved by determining the intensity parameters that minimize the root mean-squared variation between the experimentally measured and theoretically calculated integrated absorption coefficient. In addition, we neglected the magnetic dipole contribution to the transition probability.

By using the Judd-Ofelt intensity parameters, the spontaneous emission probability *A(J,J')* for a particular transition $SLJ \rightarrow S'L'J'$ can be calculated from

$$A(J,J') = \frac{64\pi^4 e^2}{3h(2J+1)} \frac{n(n^2+2)^2 \bar{\nu}^3}{9} \times \sum_{t=2,4,6} \Omega_t \left| \left\langle SLJ \left\| U^{(t)} \right\| S'L'J' \right\rangle \right|^2 \qquad 3.3.1.2$$

where $\bar{\nu}$ is the mean wavenumber of the transition. The radiative lifetime (τ_R) for the J^{th} excited state is equal to the inverse of the total spontaneous emission probability for the transitions originating from that state to all possible *J'* states and can be expressed as

$$\tau_R = \frac{1}{\sum_{J'} A(J,J')} \qquad 3.3.1.3$$

The best-fit values of the Judd- Ofelt intensity parameters Ω_2 , Ω_4 , Ω_6 , and the resulting radiative lifetimes are shown in the Table 3.3.1.1.

Tm_2O_3 concentrations	Ω_2 (10^{-20} cm^2)	Ω_4 (10^{-20} cm^2)	Ω_6 (10^{-20} cm^2)
0.125 mol.%	3.77	0.41	0.83
0.25 mol.%	4.27	0.42	0.84
0.5 mol.%	4.51	0.82	0.88
1.0 mol.%	4.51	0.76	1.13

Table. 3.3.1.1 Judd-Ofelt intensity parameters for the 1460-nm and 1860-nm bands at different Tm_2O_3 concentrations.

In the radiative lifetime calculations for the $^3H_4$ and $^3F_4$ levels, we used Judd-Ofelt intensity parameters of the 1 mol.% doped sample at which signal to noise ratio is better. The average radiative lifetimes were then determined as 2.57±0.20 ms and 0.35±0.01 ms for the $^3H_4$ and $^3F_4$ levels, respectively. In the decay of the $^3F_4$ level, transitions to three lower energy states, namely $^3H_5$, $^3H_4$, and $^3H_6$, are involved. As can be seen from Table 3.3.1.2 which shows the branching ratios from the $^3F_4$ level, the transitions $^3F_4 \rightarrow {}^3H_4$ and $^3F_4 \rightarrow {}^3H_5$ have only small contributions.

TeO_2-K_2O-Nb_2O_5	β ($^3F_4$→)		
	$^3H_5$	$^3H_4$	$^3H_6$
Tm_2O_3 concentrations			
1.0 mol.%	0.010	0.079	0.911
0.5 mol.%	0.010	0.081	0.910
0.25 mol.%	0.010	0.080	0.911
0.125 mol.%	0.010	0.082	0.908

Table. 3.3.1.2 Calculated branching ratios β of the $^3F_4$ level.

3.3.2 Fluorescence Spectroscopy

Figure 3.3.2.1 shows the emission spectra of the two transitions of Tm^{3+} ion originating from $^3F_4$ and $^3H_4$ levels to the ground level for two glass samples having Tm_2O_3 concentrations of 0.5 and 1.0 mol.%. These bands are centered near to 1460 nm and 1860 nm, respectively.

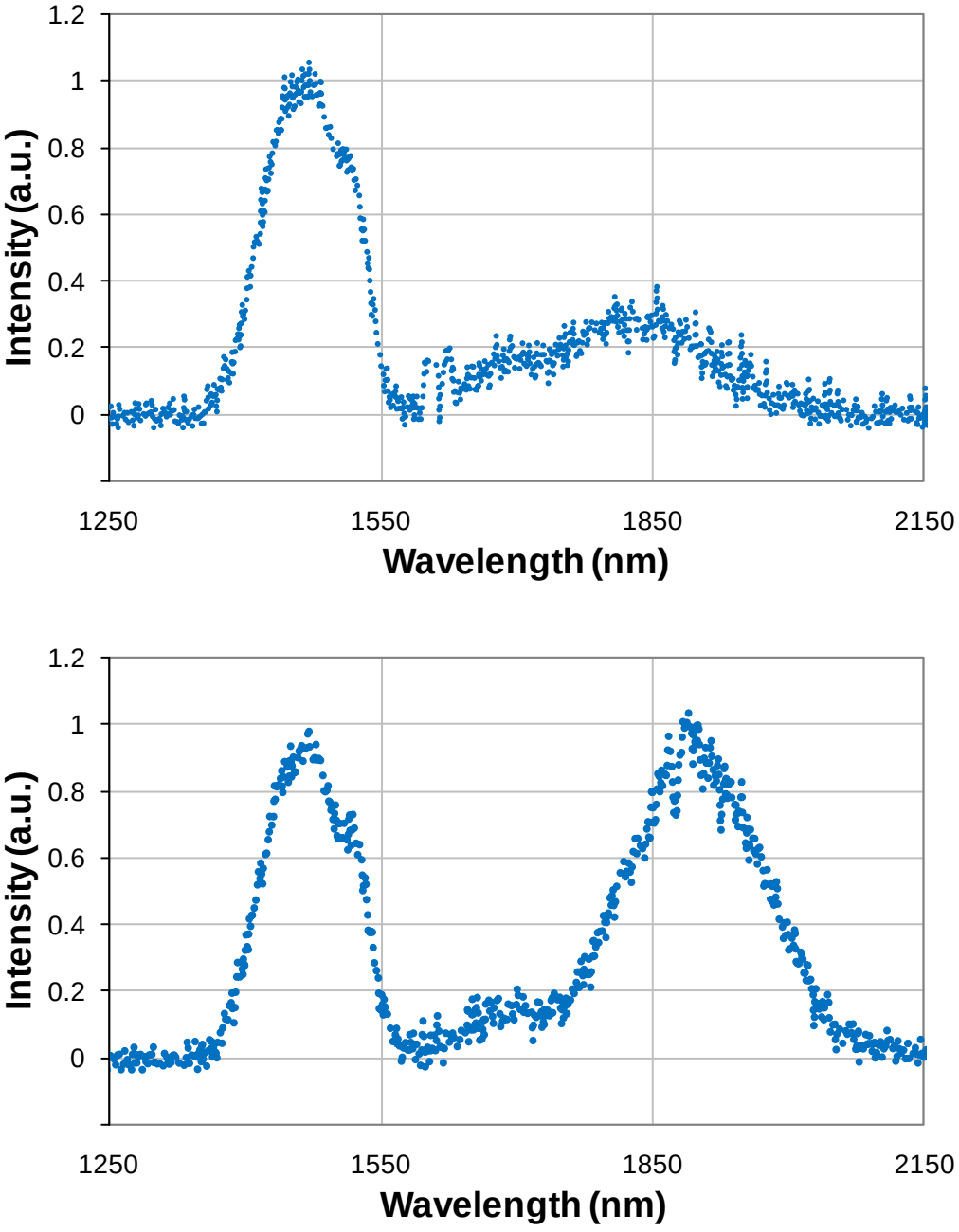

Fig. 3.3.2.1 Emission spectra of the two transitions of Tm^{3+} ion originating from $^3F_4$ and $^3H_4$ levels to the ground level for two glass samples having Tm_2O_3 concentrations of 0.5 and 1 mol.%, respectively.

As can be seen, the increase of the ion concentration results in the enhancement of 1860 nm emission band due to cross relaxation which is commonly observed in Tm^{3+} doped systems [34-35] . Cross relaxation is a nonradiative energy transfer process which occurs when an excited ion in the upper energy state decays to an intermediate energy level and transfers its energy non-radiatively to a nearby ion in the ground state. As a result, the neighboring ion in the ground state also makes a transition to the intermediate state. By this way, it is possible to obtain two excited ions in the intermediate level by absorption of only one pump photon. In this particular case, the mechanism can be described as $^3H_6 \rightarrow {}^3H_4$; $^3F_4 \rightarrow {}^3H_4$.

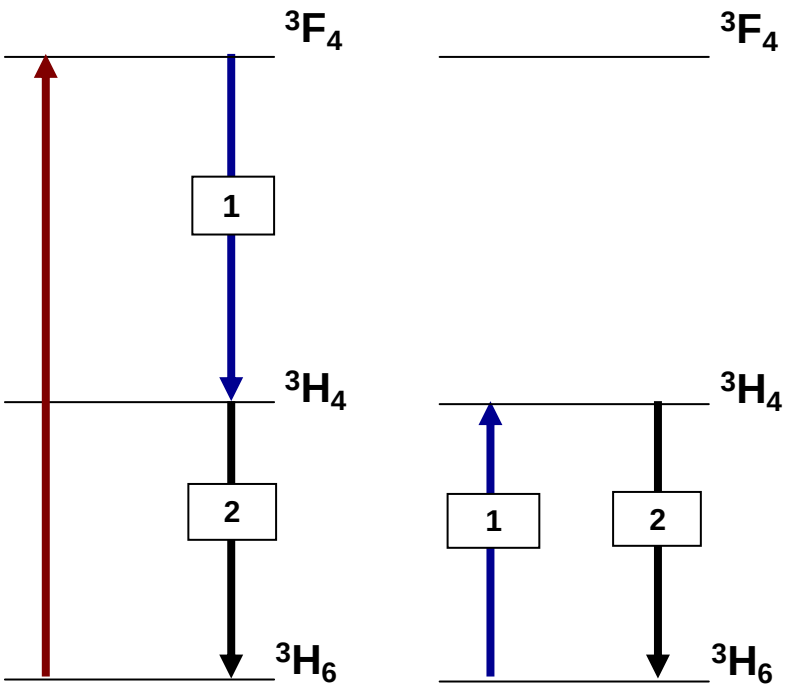

Fig. 3.3.2.2 Energy-level diagram of Tm^{3+} ions showing cross-relaxation mechanism

As a consequence, radiative decay of these ions may result in emission of two photons near 1860 nm. As the ion concentration increases, the cross relaxation mechanism becomes more significant and results in the enhancement of the 1860-nm band in relation to that of the 1460nm band. Figure 3.3.2.3 shows the ratio of the peak intensities at 1460 nm (I_{1460}) and 1860 nm.

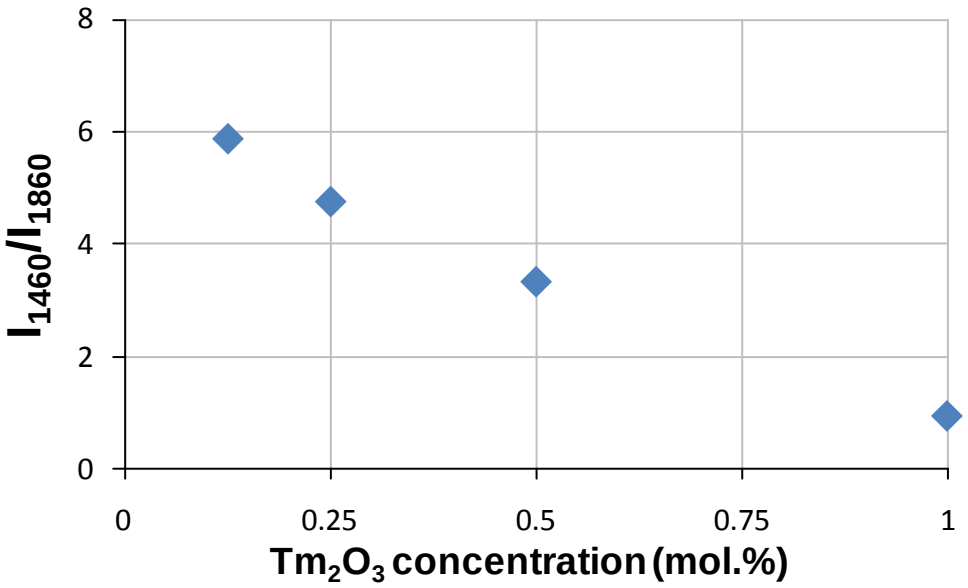

Fig. 3.3.2.3 Ratio of the peak emission intensities at 1460 nm (I_{1460}) and 1860 nm (I_{1860}) as a function of Tm_2O_3 concentration.

As can be seen, the relative strength of the 1860 nm band increases as the ion concentration increases, verifying the role of cross relaxation. Figure 3.3.2.4 shows the measured fluorescence decay signals of the $^3F_4$ and $^3H_4$ levels for two glass samples having 0.125 and 1 mol. % Tm_2O_3 concentration.

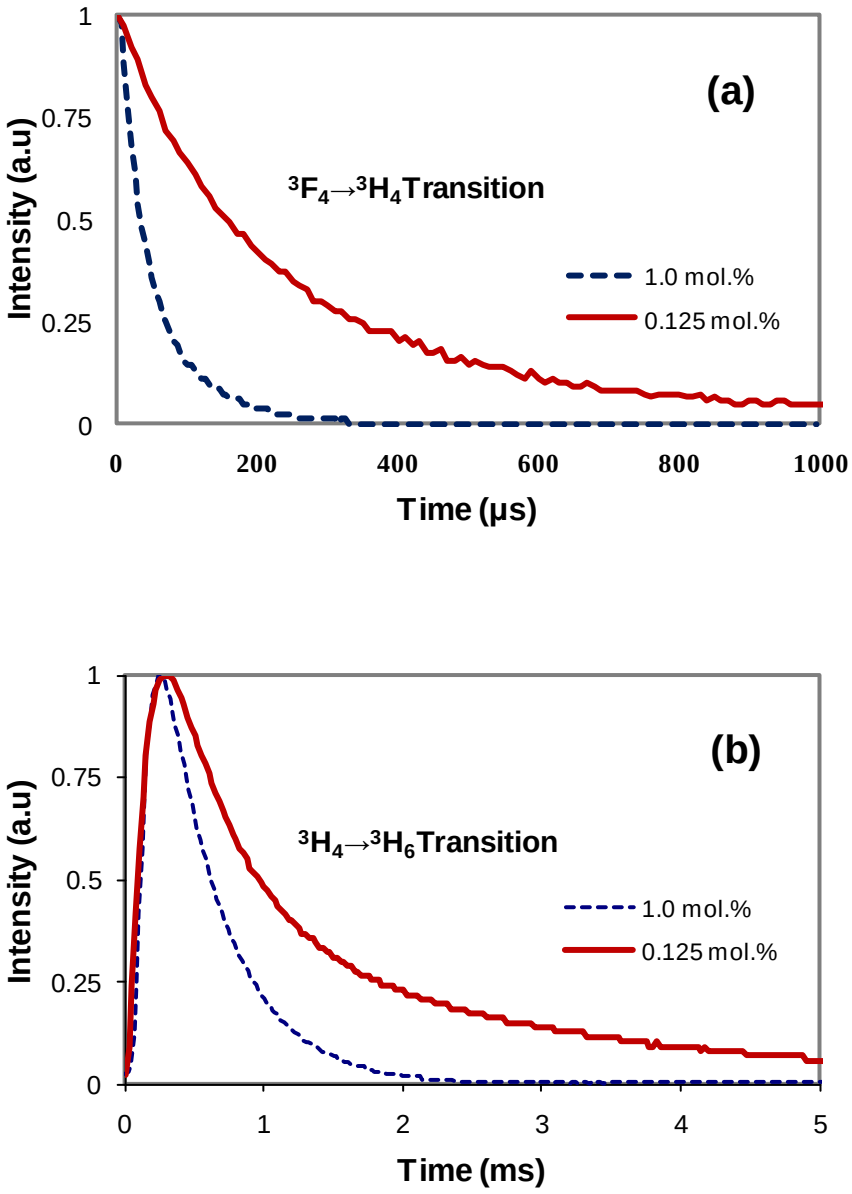

Fig. 3.3.2.4 Measured fluorescence decay curves of the (a) $^3F_4$ level and (b) $^3H_4$ level for the two Tm_2O_3: TeO_2 -K_2O-Nb_2O_5 samples having Tm_2O_3 concentrations of 1.0 and 0.125 mol.%.

The fluorescence lifetimes (τ_F) were obtained by fitting an exponential to the tail of the measured signal where the initial nonlinear effects due to cross relaxation and pumping are insignificant. With increasing Tm_2O_3 concentration from 0.125 mol. % to 1.0 mol. %, we observed a decrease in the fluorescence lifetime from 814 μs to 439 μs ($^3H_4$ level) and from 258 μs to 47 μs ($^3F_4$ level). From the calculated radiative lifetimes and experimentally measured fluorescence lifetimes, the luminescence quantum efficiency (η) can then be determined by using $\eta = \tau_F / \tau_R$. Table 3.3.2.1 summarizes the obtained fluorescence lifetimes and quantum efficiencies of the glass samples for two transitions.

TeO_2-K_2O-Nb_2O_5	τ_F (μs)		η (%)	
	$^3H_4$	$^3F_4$	$^3H_4$	$^3F_4$
Tm_2O_3 concentrations				
0.125 mol.%	814	258	32	74
0.25 mol.%	572	199	22	57
0.5 mol.%	545	148	21	43
1.0 mol.%	439	47	17	14

Table. 3.3.2.1 Measured fluorescence lifetimes and the corresponding luminescence quantum efficiencies of the Tm_2O_3: TeO_2-K_2O-Nb_2O_5 samples for the $^3H_4$ and $^3F_4$ bands at different concentrations.

The highest quantum efficiencies for 1460 nm (74 %) and 1860 nm (32 %) emission bands were obtained with the sample having 0.125 mol. % Tm_2O_3 concentration. As shown in the Table 3.3.2.1, smaller quantum efficiencies at higher ion concentrations suggest an increase in the nonradiative relaxation mechanisms.

Emission spectra data were also used to determine the emission cross section (σ_{em}) of the glass samples. The emission cross section was found by using the Fuchtbauer-Ladenburg formulation [36-37],

$$\sigma_{em}(\lambda) = \frac{\lambda^5 I(\lambda) A(J, J')}{8\pi n^2 c \int I(\lambda)\lambda d\lambda} \qquad 3.3.2.4$$

where $I(\lambda)$ is the normalized fluorescence intensity at the wavelength λ. In Table 3.3.2.2, emission cross sections for two emission bands of the tellurite glasses at different Tm_2O_3 concentrations are shown.

Tm_2O_3 concentrations	σ_{em} (10^{-21} cm^2)	
	1460 nm	1860nm
1.0 mol.%	2.67	5.61
0.5 mol.%	2.74	6.12
0.25 mol.%	2.40	5.46
0.125 mol.%	3.00	6.85
Average	2.70	6.01

Table. 3.3.2.2 Emission cross sections for the 1460-nm and 1860-nm bands of the Tm^{3+}:TeO_2-K_2O-Nb_2O_5 glass at different Tm_2O_3 concentrations.

The average emission cross sections were determined to be 2.7×10^{-21} and 6.01×10^{-21} cm^2 for 1460 and 1860 nm bands, respectively. These results compare well with values reported for other tellurite hosts [9, 38].

3.4 Conclusion

We have conducted a detailed spectroscopic characterization of the Tm^{3+} doped host Tm^{3+}:TeO_2-K_2O-Nb_2O_5 at different active ion concentrations by using the Judd-Ofelt analysis. By performing a Judd-Ofelt analysis of the absorption bands, we obtained average radiative lifetimes of 2.57±0.20 ms and 0.35±0.01 ms for the $^3H_4$ and $^3F_4$ levels, respectively. Furthermore, we also observed that an increase in the Tm_2O_3 concentration from 0.125 mol. % to 1.0 mol. % results in a decrease of the measured fluorescence lifetime from 814 to 439 μs and from 258 to 47 μs for the $^3H_4$ and $^3F_4$ levels, respectively, due to stronger non-radiative decay. The highest quantum efficiency of 32 % was obtained for the sample doped with 0.125 mol. % Tm_2O_3 for the $^3H_4$ level. Results show that cross relaxation becomes important as the ion concentration is increased, leading to the quenching of the 1460-nm band and enhancement of the 1860-nm emission. The highest emission cross section of 6.85×10^{-21} cm^2 measured for the 1860-nm band reveals the potential of this host for the development of 2-μm lasers in bulk glass as well as fiber media.

Chapter 4: Tm^{3+}:TeO_2 Glasses with Different Host Compositions

4.1 Introduction

This chapter is dedicated to the spectroscopic characterization of the two new tellurite based glass hosts prepared at different ion concentrations. Judd-Ofelt theory was used in the analysis of the experimental data as we did in the previous chapter. However, the main emphasis of this chapter is not to discuss the same Judd-Ofelt analysis or describe the experimental methods in the fluorescence measurements once again. Rather, I will try to make a comparative analysis on the spectroscopic characteristics (i.e. cross sections and luminescence quantum yields) of the tellurite based hosts with different glass modifiers.

Two tellurite based glass samples were prepared by using niobium-oxide as a glass modifier: $(1.0)Tm_2O_3$: $(95)TeO_2$ - (4) Nb_2O_5 (TeNbTm1) , and $(0.25)Tm_2O_3$: $(95)TeO_2$ - (4.75) Nb_2O_5 (TeNbTm025) , and four samples were prepared at different concentrations using zinc-oxide as a glass modifier: $(1.0)Tm_2O_3$: $(80)TeO_2$ – (19) ZnO (TeZnTm1), $(0.5)Tm_2O_3$: $(80)TeO_2$ – (19.5) ZnO (TeZnTm05) , $(0.25)Tm_2O_3$: $(80)TeO_2$ – (19.75) ZnO

(TeZnTm025) , and (0.125)Tm_2O_3 : (80)TeO_2 – (19.875)ZnO (TeZnTm0125) . The measurements were conducted at different Tm^{3+} ion concentrations for the two emission bands with peaks at 1460 nm ($^3F_4$ level) and 1860 nm ($^3H_4$ level).

4.2 Experimental Results and Discussion

4.2.1 Absorption Analysis

Remember, the contribution of the electric-dipole transition to the integrated absorption coefficient for the rare earth ions can be obtained by using the equation [28-29],

$$\Sigma_{\mu}{}_{calc} = \frac{8\pi^3 e^2}{3ch}\frac{(n^2+2)^2}{9n}\frac{\bar{\lambda}}{(2J+1)}N_o \times \sum_{t=2,4,6}\Omega_t \left|\left\langle SLJ\left\|U^{(t)}\right\|S'L'J'\right\rangle\right|^2 \quad 4.2.1.1$$

Approximate values for Judd-Ofelt intensity parameters appearing in Eq. (4.2.1.1) can be found by using the experimentally measured integrated absorption coefficient $(\Sigma_\mu)_{exp}$ and the matrix elements $U^{(t)}$ reported in Ref. [22]. Here as an example, we provided the Fig. 4.2.1.1 showing the measured absorption spectra of two TeNbTm glass samples which have Tm_2O_3 concentrations of 0.25 and 1 mol. %.

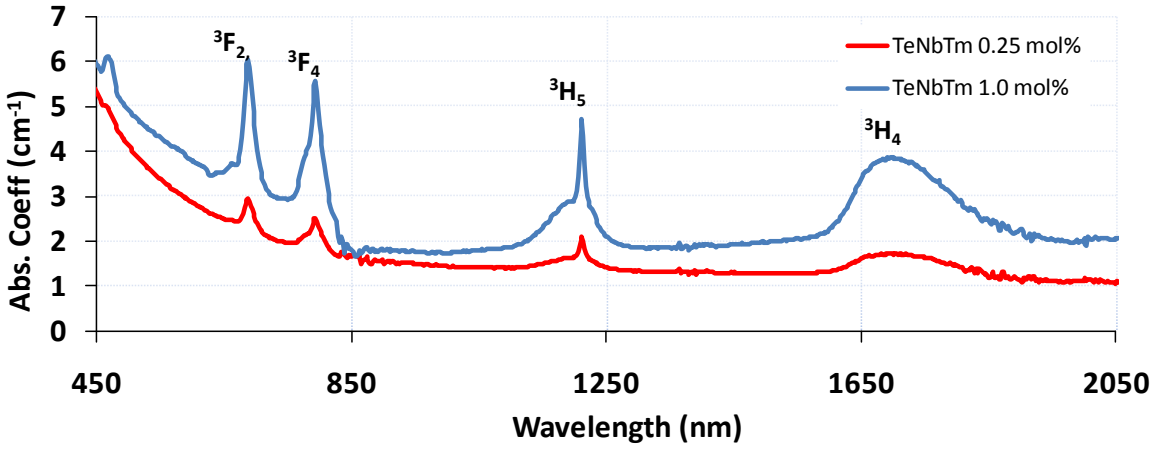

Fig. 4.2.1.1 Measured absorption spectra of two TeNbTm glass samples which have Tm_2O_3 concentrations of 0.25 and 1 mol. %.

In our analysis, we used four ground state absorption bands of Tm^{3+} ion to the $^3F_{2,3}$, $^3F_4$, $^3H_5$, $^3H_4$ levels (see Fig.4.2.1.1) to determine the intensity parameters as well as the radiative lifetimes. The equation was solved by determining the intensity parameters that minimize the root mean-squared variation between the experimentally measured and theoretically calculated integrated absorption coefficient. Table 4.2.1.1 summarizes the theoretically calculated and experimentally measured integrated absorption coefficients and root mean-squared errors for all of the tellurite glass samples.

Tenbktm	1.0 mol. % sample		0.5 mol. % sample	
Transition from $^3H_6$→	$(\Sigma\mu)$ exp (10^{-6})	$(\Sigma\mu)$ calc (10^{-6})	$(\Sigma\mu)$ exp (10^{-6})	$(\Sigma\mu)$ calc (10^{-6})
$^3F_{2,3}$	4.57	6.07	1.66	2.62
$^3F_4$	7.84	8.56	3.57	4.04
$^3H_5$	11.8	9.8	5.85	4.57
$^3H_4$	33.56	33.69	17.1	17.18
σ_{rms} (10^{-6})	1.30		0.83	
	0.25 mol. % sample		0.125 mol. % sample	
	$(\Sigma\mu)$ exp (10^{-6})	$(\Sigma\mu)$ calc (10^{-6})	$(\Sigma\mu)$ exp (10^{-6})	$(\Sigma\mu)$ calc (10^{-6})
$^3F_{2,3}$	0.82	1.12	0.34	0.55
$^3F_4$	1.74	1.89	0.77	0.87
$^3H_5$	2.42	2.02	1.23	0.96
$^3H_4$	7.48	7.51	3.38	3.40
σ_{rms} (10^{-6})	0.26		0.18	

Tezntm	1.0 mol. % sample		0.5 mol. % sample	
Transition from $^3H_6$→	$(\Sigma\mu)$ exp (10^{-6})	$(\Sigma\mu)$ calc (10^{-6})	$(\Sigma\mu)$ exp (10^{-6})	$(\Sigma\mu)$ calc (10^{-6})
$^3F_{2,3}$	6.27	7.53	3.64	3.84
$^3F_4$	9.04	9.65	4.68	4.78
$^3H_5$	13.25	11.55	6.01	5.74
$^3H_4$	38.50	38.61	17.70	17.72
σ_{rms} (10^{-6})	1.10		0.18	
	0.25 mol. % sample		0.125 mol. % sample	
	$(\Sigma\mu)$ exp (10^{-6})	$(\Sigma\mu)$ calc (10^{-6})	$(\Sigma\mu)$ exp (10^{-6})	$(\Sigma\mu)$ calc (10^{-6})
$^3F_{2,3}$	1.91	2.16	0.34	0.55
$^3F_4$	2.03	2.15	0.77	0.87
$^3H_5$	3.36	3.03	1.23	0.96
$^3H_4$	9.80	9.82	3.38	3.4
σ_{rms} (10^{-6})	0.22		0.18	

Tenbtm	1.0 mol. % sample		0.25 mol. % sample	
Transition from $^3H_6$→	$(\Sigma\mu)$ exp (10^{-6})	$(\Sigma\mu)$ calc (10^{-6})	$(\Sigma\mu)$ exp (10^{-6})	$(\Sigma\mu)$ calc (10^{-6})
$^3F_{2,3}$	6.29	6.35	1.38	1.54
$^3F_4$	8.71	8.74	1.73	1.81
$^3H_5$	10.00	9.93	2.58	2.36
$^3H_4$	32.90	32.90	8.85	8.86
σ_{rms} (10^{-6})	0.05		0.14	

Table. 4.2.1.1 Theoretically calculated and experimentally measured integrated absorption coefficients and root mean-squared errors for all of the tellurite glass samples at different concentrations

As can be seen from the table, errors stay in an acceptable margin. By using integrated absorption coefficients $(\Sigma_\mu)_{exp}$ inside Eq. 4.2.1.1 we obtained approximate solution for the system of four equations involving the three Judd-Ofelt intensity parameters. Table 4.2.1.2 summarizes the resulting JO intensity parameters for three different glass host prepared at different ion concentrations.

Judd-Ofelt Intensity Parameters	Ω_2	Ω_4	Ω_6
	(10^{-20} cm^2)	(10^{-20} cm^2)	(10^{-20} cm^2)
TeNbKTm			
0.125 mol%	3.77	0.41	0.83
0.25 mol%	4.27	0.42	0.84
0.5 mol%	4.51	0.82	0.88
1.0 mol%	4.51	0.76	1.13
TeZnTm			
0.125 mol%	3.66	1.96	1.10
0.25 mol%	2.86	1.81	1.06
0.5 mol%	3.74	0.72	1.21
1.0 mol%	4.02	0.93	1.12
TeNbTm			
0.25 mol%	3.21	1.75	0.76
1.0 mol%	4.09	0.69	1.11

Table. 4.2.1.2 JO intensity parameters for three different glass host prepared at different ion concentrations

From the table, it can be seen that values of JO intensity parameters differs for the samples with different host compositions resulting in deviations in the calculated radiative lifetimes. In the radiative lifetime calculations for the $^3H_4$ and $^3F_4$ levels, we used Judd-Ofelt intensity parameters of the 1 mol.% doped samples where the signal to noise ratio is the highest. The average radiative lifetimes was obtained as 2.76 ms and 0.37 ms for the sample TeNbTm , and 2.57 ms and 0.35 ms for the sample TeNbKTm, and for the sample containing zinc as a modifier (TeZnTm), we obtained smaller average radiative lifetime 2.55 ms for the $^3H_4$ and $^3F_4$ levels, respectively . In the decay of the $^3F_4$ level, transitions to

three lower energy states, namely $^3H_5$, $^3H_4$, and $^3H_6$, are involved. As can be seen from Table 4.2.1.3 which shows the branching ratios from the $^3F_4$ level, the transitions $^3F_4 \rightarrow {}^3H_4$ and $^3F_4 \rightarrow {}^3H_5$ have only small contributions for all tellurite hosts.

Branching ratios	β ($^3F_4 \rightarrow$)		
	$^3H_5$	$^3H_4$	$^3H_6$
TeNbKTm			
1.0 mol%	0.010	0.079	0.911
0.5 mol%	0.010	0.081	0.910
0.25 mol%	0.010	0.080	0.911
0.125 mol%	0.010	0.082	0.908
TeZnTm			
1.0 mol%	0.012	0.079	0.909
0.5 mol%	0.012	0.079	0.909
0.25 mol%	0.012	0.079	0.909
0.125 mol%	0.012	0.079	0.909
TeNbTm			
1.0 mol%	0.010	0.078	0.913
0.25 mol%	0.010	0.077	0.913

Table. 4.2.1.3 The branching ratios from the $^3F_4$ level

4.2.2 Emission Spectroscopy

Figure 4.2.2.1 shows the emission spectra of the two transitions of Tm^{3+} ion originating from $^3F_4$ and $^3H_4$ levels to the ground level for two glass host TeZnTm having Tm_2O_3 concentrations of 1.0 and 0.25 mol.%.

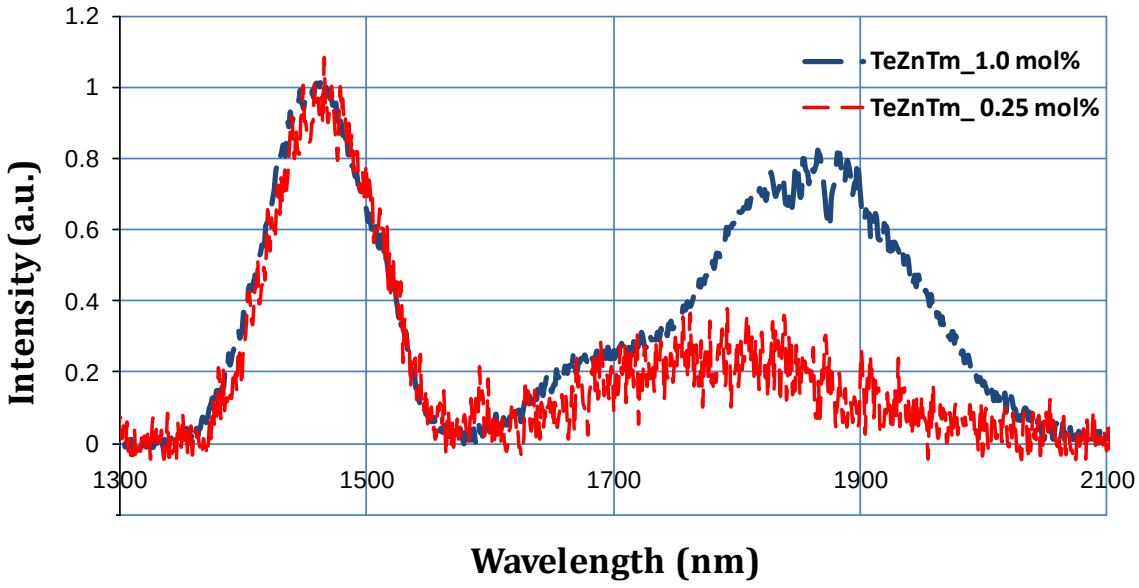

Fig. 4.2.2.1 Emission spectra of the two transitions of Tm^{3+} ion originating from $^3F_4$ and $^3H_4$ levels to the ground level for two glass host TeZnTm having Tm_2O_3 concentrations of 1.0 and 0.25 mol.%.

The emission spectrum clearly shows the two emission bands centered around 1860 nm and 1460 nm and further verifies that the role of cross relaxation becomes important at high ion concentrations leading the quenching of 1460 nm emission resulting in the enhancement of the 1860 nm emission band.

We measured the fluorescence decay signal of the $^3H_4$ level and $^3F_4$ level corresponding 1860 nm and 1460 nm transitions. The fluorescence lifetimes (τ_F) were obtained by fitting an exponential to the tail of the measured signal using Labview software. Figure shows the tails of the fluorescence decay curves for the new samples with different compositions and Tm_2O_3 concentrations for the $^3H_4$ level only.

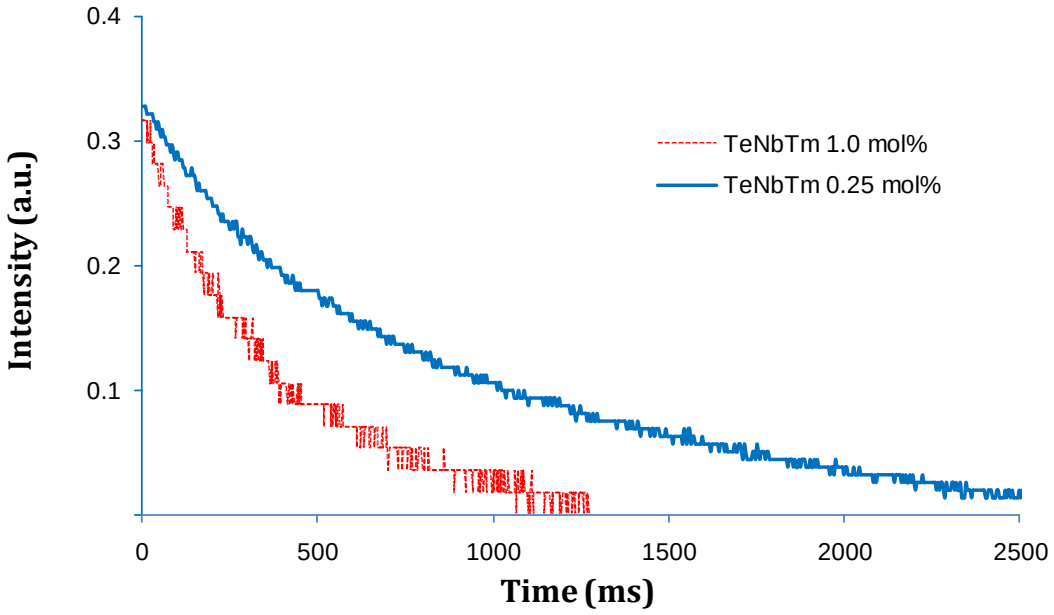

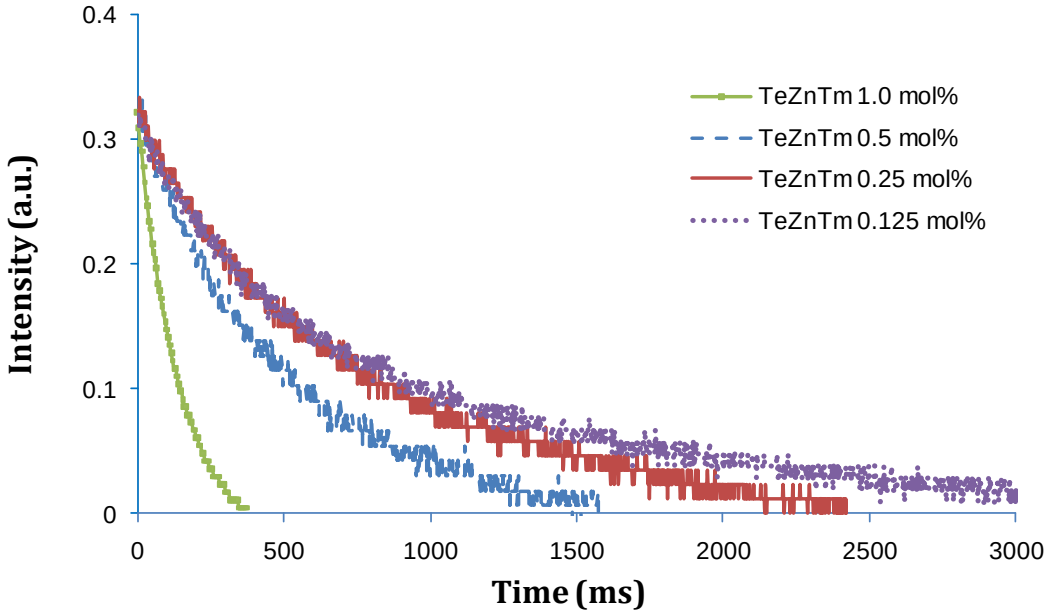

Fig. 4.2.2.2 Measured fluorescence decay curves for the TeNbTm and TeZnTm samples with different Tm_2O_3 concentrations from the $^3H_4$ level.

With increasing Tm_2O_3 concentration from 0.125 mol. % to 1.0 mol. %, we observed a decrease in the fluorescence lifetime due to the increasing role of nonradiative relaxation mechanisms. From the calculated radiative lifetimes and experimentally measured fluorescence lifetimes, the luminescence quantum efficiency (η) can then be determined by using $\eta = \tau_F / \tau_R$. Table 4.2.2.1 summarizes the obtained fluorescence lifetimes and quantum efficiencies of the glass samples for two transitions corresponding to 1860 nm and 1460 nm.

Fluorescence & radiative lifetimes and quantum yields	τ_F (μs)		η (%)		$\tau_{R\ averaged}$ (μs)	
	$^3H_4$	$^3F_4$	$^3H_4$	$^3F_4$	τ_R (1860)	τ_R (1460)
TeNbKTm	1860nm	1460nmm	1860nm	1460nm	(ms)	(ms)
0.125 mol%	814	258	32	74	2.57	0.35
0.25 mol%	572	199	22	57		
0.5 mol%	545	148	21	43		
1.0 mol%	439	47	17	14		
TeZnTm					τ_R (1860)	τ_R (1460)
0.125 mol%	806	327	32	89	2.55	0.37
0.25 mol%	722	250	28	68		
0.5 mol%	511	171	20	47		
1.0 mol%	145	35	6	10		
TeNbTm					τ_R (1860)	τ_R (1460)
0.25 mol%	893	284	32	76	2.76	0.37
1.0 mol%	382	76	14	20		

Table. 4.2.2.1 Measured fluorescence and calculated radiative lifetimes for two transitions corresponding 1860 nm and 1460 nm.

From the table, we can see that highest quantum efficiency for the sample TeZnTm was obtained as 32% for the 1860 nm emission band and 89% for the 1460 nm emission band when the ion concentration is 0.125 mol.%. For the sample TeNbTm, we reported highest obtained quantum yields as 32% and 76% for the 1860 and 1460 nm emission bands, respectively when the ion concentration was 0.25 mol.%. Emission spectra data were also used to determine the emission cross section (σ_{em}) of the glass samples. As we

did earlier, the emission cross section can be obtained by using the Fuchtbauer-Ladenburg equation [36-37],

$$\sigma_{em}(\lambda) = \frac{\lambda^5 I(\lambda) A(J, J')}{8\pi n^2 c \int I(\lambda)\lambda d\lambda} \qquad 4.2.2.2$$

In Table 4.2.2.2, emission cross sections for two emission bands of the tellurite glasses at different Tm_2O_3 concentrations are shown.

Stimulated Emission Cross Sections	σ_{em} (10^{-21} cm^2)	
	1460 nm	1860nm
TeNbKTm		
1.0 mol%	2.67	5.61
0.5 mol%	2.74	6.12
0.25 mol%	2.40	5.46
0.125 mol%	3.00	6.85
Average	2.70	6.01
TeZnTm		
1.0 mol%	2.74	5.48
0.5 mol%	2.52	5.65
0.25 mol%	2.91	6.85
0.125 mol%	2.95	7.36
Average	2.78	6.33
TeNbTm		
1.0 mol%	2.65	4.99
0.25 mol%	2.60	6.28
Average	2.62	5.63

Table. 4.2.2.2 Emission cross sections for the 1460-nm and 1860-nm bands of the Tm^{3+}:TeO_2 based glass hosts at different Tm_2O_3 concentrations.

For the TeNbTm sample, we obtained $2.62x10^{-21}$ and $5.63x10^{-21}$ cm^2 average stimulated emission cross sections for the 1460 and 1860 nm bands respectively. It can be further seen from the table, for the sample containing zinc as a glass modifier (TeZnTm), the average emission cross sections were determined to be $2.78x10^{-21}$ and $6.33x10^{-21}$ cm^2 for 1460 and 1860 nm bands, respectively. These results compare well with values reported for other tellurite hosts [9, 38] and it can also be concluded that for the TeZnTm sample, we obtained higher stimulated emission cross sections (as high as $7.36x10^{-21}$) especially for the 1860 nm emission band.

4.3 Conclusion

In this part we have conducted the same spectroscopic analysis on two new types of tellurite glass hosts [Tm_2O_3: TeO_2 - ZnO (**TeZnTm**) and Tm_2O_3: TeO_2 - Nb_2O_5 (**TeNbTm**)] in order to investigate the effect of host composition on the cross sections and the luminescence quantum efficiencies. Judd Ofelt intensity parameters which relate absorption bands to the transition strengths for the particular transitions are expected to exhibit weak dependence on the host composition. From the data, it can be concluded that Judd-Ofelt intensity parameters vary slightly among tellurite glasses with different compositions as expected. Yet, our calculations showed that for the sample containing zinc as a glass modifier **TeZnTm** we obtained shorter radiative lifetimes for the transition

corresponding 1860 nm band. We obtained average radiative lifetime 2.55±0.07 ms for the TeZnTm samples and 2.76 ±0.03 ms for the TeNbKTm samples for the $^3H_4$ level.

From the lifetime measurements and the radiative lifetime calculations using Judd Ofelt theory, we obtained luminescence quantum efficiencies of the samples. Highest quantum efficiency for the sample TeZnTm was 32% for the 1860 nm emission band and 89% for the 1460 nm emission band. For the sample TeNbTm we reported highest obtained quantum yields as 32% and 76% for the 1860 and 1460 nm emission bands respectively.

As we discussed earlier, cross relaxation mechanism is a nonradiative energy transfer process which is quite common for the thulium system. For our purpose, contribution of the cross relaxation which favors 2 μm emission is desirable. For all of the samples, we observed the effect of cross relaxation which becomes significant at high ion concentrations leading the quenching of the 1460 nm emission band and results in the enhancement of the 1860 nm emission.

Samples with the low concentration provide higher quantum efficiencies favorable for our purposes but on the other hand their absorptions are weak. When we increase the ion concentration, quantum efficiencies decrease but absorption together with the cross relaxation for the 1860 nm band will compensate. It is important to find an optimum here where there is not dramatically low quantum yield and pump absorption.

0.25 or 0.5 mol% samples may be used as the laser gain media. And weak absorption problem for the low concentration samples can partially be handled using double pumping which increases effective absorption of the sample.

Stimulated emission cross sections are also important optical parameters from which one can conclude the potential of the new materials for the laser applications. For the TeNbTm sample, we obtained 2.62×10^{-21} and 5.63×10^{-21} cm^2 emission cross sections for the 1460 and 1860 nm bands respectively. For the sample containing zinc as a glass modifier (TeZnTm), the average emission cross sections were determined to be 2.78×10^{-21} and 6.33×10^{-21} cm^2 for 1460 and 1860 nm bands, respectively.

These results compare well with values reported for other tellurite hosts [9, 38] and it can also be concluded that for the TeZnTm sample we obtained higher stimulated emission cross sections (as high as 7.36×10^{-21}) especially for the 1860 nm emission band. Together with the other hosts we analyzed, TeZnTm glass are good candidates for the development of 2-μm lasers with high emission cross sections for the 1860-nm band.

Chapter 5: Lasing Trials with the Thulium Doped Tellurite Glasses

In this thesis work, we have conducted detailed experiments in order to investigate spectroscopic characteristics of new types of thulium doped tellurite based glass hosts primarily for 2μm laser applications. Results of the Judd-Ofelt analysis together with the fluorescence spectroscopy showed that these new types of thulium tellurite hosts are good candidates for laser applications near 2μm as bulk glass as well as fibers. In this chapter, we will summarize our lasing trials with the thulium doped tellurite glasses.

In the literature, lasing from bulk TZN and TZNG (tellurium, zinc, sodium, (germanium)) glasses was demonstrated with slope efficiencies up to 28% and with the maximum output powers of 124 mW. TZNG glass also offers 135 nm tunability range from 1830 nm to 2025 nm [20]. In 2010, continuous wave operation was demonstrated with a bulk TZNG glass pumped by a SDL (semiconductor disk laser) at 1211 nm [39]. Recently, mode-locked operation of bulk Tm^{3+} - Ho^{3+} codoped TZN tellurite glass together with thulium doped fluorogermanate glass was reported [21]. They obtained 630-fs pulses with 38 mW of

average power from Tm^{3+} - Ho^{3+} codoped TZN tellurite glass operating at 2012 nm with the help of a SESAM (semiconductor saturable absorber mirror).

5.1 Experimental

5.1.1 Pump Source

As an excitation source, we employed a homemade tunable Ti:sapphire laser pumped with Nd:YAG + KTP system. Our pump laser produced 60 ns pulses at a repetition rate of 1 kHz. It was tuned to operate around 800 nm where the tellurite glass samples have the maximum absorption for this particular transition. In Fig. 5.1.1.1, the standard x-cavity Ti: sapphire pump laser is shown.

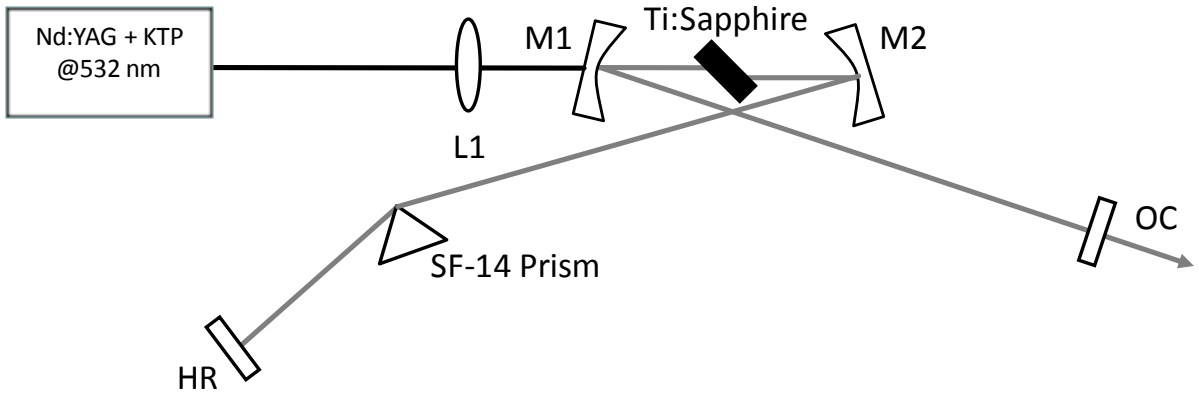

Fig. 5.1.1.1 Schematic of the homemade tunable Ti:sapphire cavity

As a rule of thumb, mirrors in the cavity are chosen to be coated such that they are high reflectors at the laser wavelengths (800 nm) and highly transmitting at the pump wavelength (532 nm) with low loss. We can tune the wavelength of the Ti: sapphire laser with the help of an SF-14 prism and the mirror set we used inside the cavity determines the tuning range. In the following figure, Nd:YAG+KTP system which is used to pump the Ti:sapphire crystal is also shown.

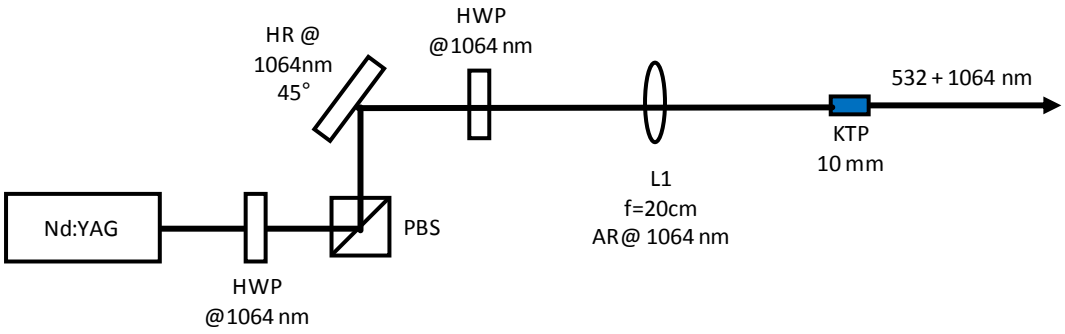

Fig. 5.1.1.2 Nd:YAG+KTP system used to pump the Ti:sapphire crystal

This system was used to convert 1064 nm produced by Nd:YAG laser to 532 nm where Ti:sapphire crystal has the maximum absorption.

5.1.2 Spot-size Measurements and Cavity Design

In order to build the cavity for the lasing experiments we need to estimate cavity dimensions based on the calculations for the best mode-matching of the pump and the laser

spot sizes. For this purpose, we measured the spot size of the pump (Ti: sapphire laser) using standard knife-edge method by assuming a Gaussian beam profile. Fig. 5.1.2.1 summarizes results of beam quality M^2, Rayleigh range z_f, and spot-size w_0 using Mathematica software from which we obtained 22.8 μm beamwaist for the pump.

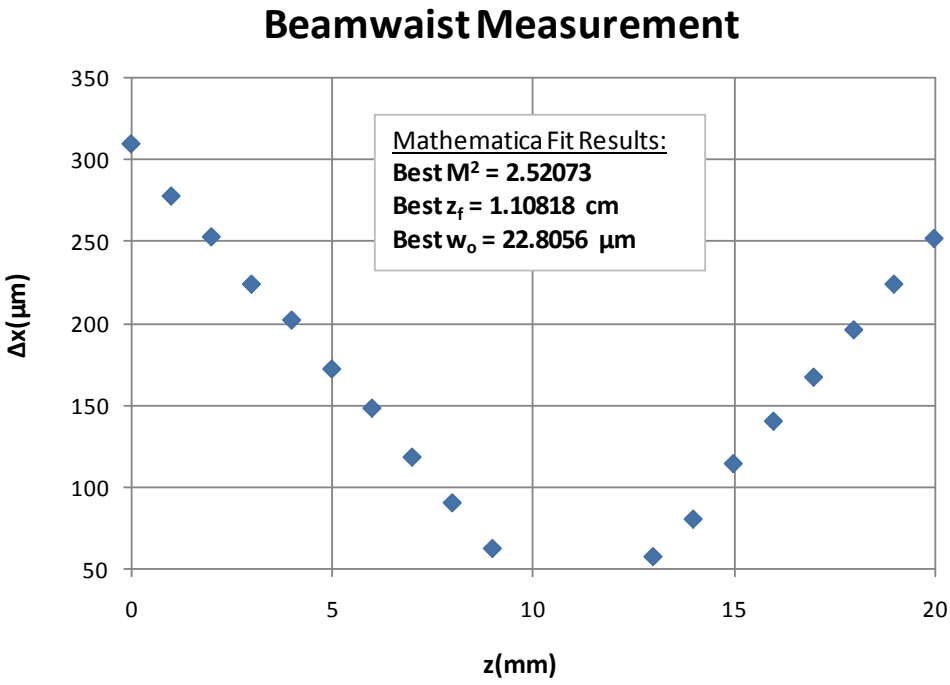

Fig. 5.1.2.1 Beam waist measurement results using the knife-edge method.

In order to determine cavity dimensions which will provide best mode-matching of pump and laser, a code written in Mathematica which analyzes simple x-cavity with specified arm lengths and mirror separations using ABCD matrix method was used. Fig

5.1.2.2, shows the cavity dimensions we choose which yield 22 μm laser beamwaist which is well-matched with the pump.

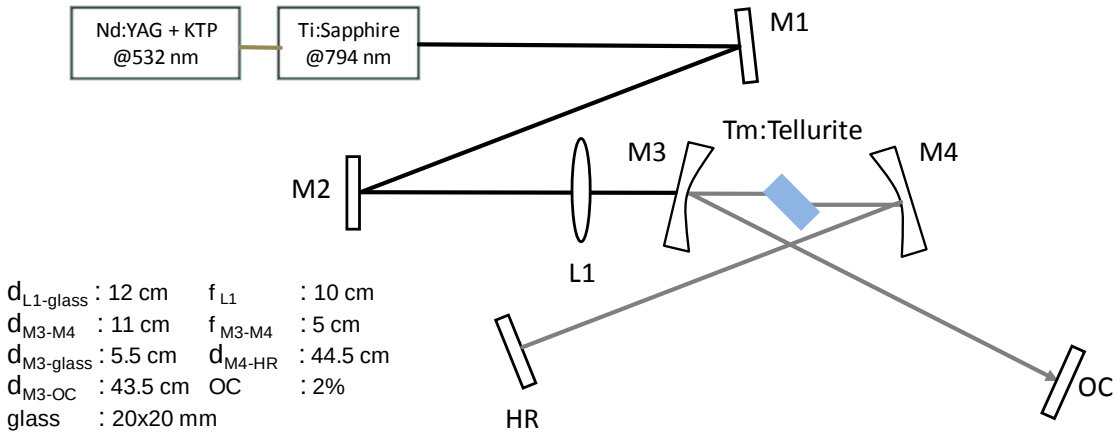

Fig. 5.1.2.2 The x-cavity designed for the lasing trials of the Tm:tellurite glasses

Using the setup which is shown in the figure above, we tried to obtain lasing from the thulium tellurite glasses with Tm_2O_3 concentration of 1.0 mol% and 0.5 mol%. In our trials, we have started with the estimated arm lengths for the cavity as a result of spot-size measurements. By slightly changing arm lengths and mirror separations, we maximized the feedback coming from the mirrors and high reflector arm to the detector (PbS) placed behind the 2% output coupler. For the glass sample with 1.0 mol% Tm_2O_3 concentration (TeNbKTm1), we went up to 250 mW of pump power (before M1) which corresponds 199 mW of absorbed power on the glass but we could not achieve lasing. We then decided to

go with the double pumping method which simply increases the effective absorption on the glasses.

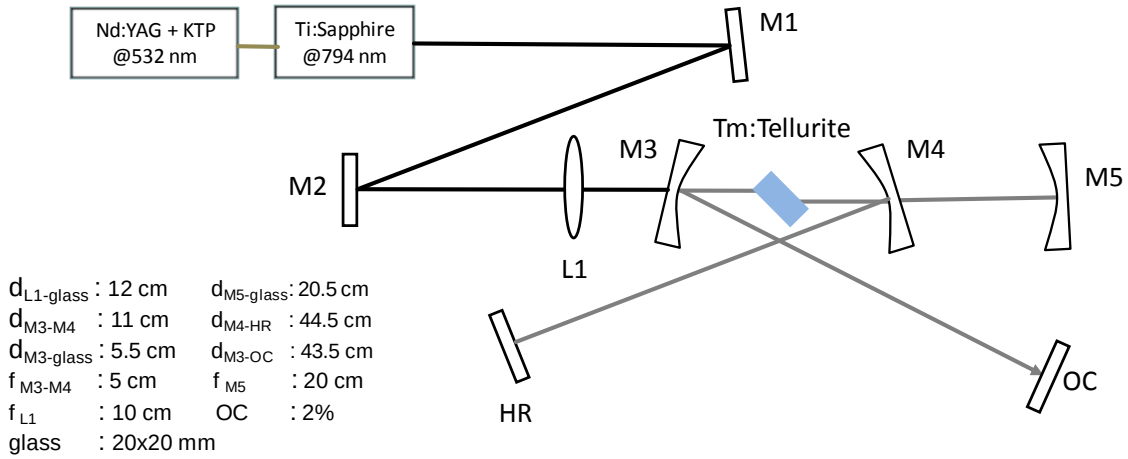

Fig. 5.1.2.3 Double pumping scheme used to increase effective absorption on the thulium doped tellurite glass

Following same routines in the allignments, we tried other samples as well (TeNbKTm05, TeNbTm1, TeNbTm025, TeZnTm1, TeZnTm05, TeZnTm025) modifying cavity dimensions such that we observe maximum feedback on the detector yet we could not obtain lasing.

5.2 Discussion

In the lasing trials with the thulium doped tellurite glasses, we mostly focused on the optimization of the cavity and choosing samples with appropriate ion concentrations based

on the results of the spectroscopic analysis we have conducted. In order to test our cavity, we inserted well-studied Tm:YAP crystal and obtained lasing performance readily, verifying the efficiency of our cavity and experimental procedures.

Apart from this discussion, there is an important issue that should be addressed during the preparation of the samples which plays a key role in the success of lasing trials: Minimizing OH^- impurities of which absorption bands coincide with the emission band of interest around 2μm.

There are several methods described in many other references suggesting solutions to the OH^- contamination issue [40-42]. In the preparation of the glass samples, purities of the starting chemicals are essential and better than 3-4 digit purity levels are required. Powders are preferred to be kept in the dry store/batch conditions and most critically should be melted in the dry O_2 atmosphere .There are also several examples offering solutions to the OH^- impurity problem like in-situ fluorination and bubbling glass sample with a gas during melting [40-41].

In the literature, lasing performance of the bulk tellurite glass was achieved [20] and continuous wave performance and mode-locked operation was demonstrated quite recently [21, 39] showing that tellurite glass family deserves great attention for the development of the lasers operating around 2 μm as bulk as well as fiber applications.

Chapter 6: Conclusions

In this thesis work, we investigated spectroscopic properties of new types of thulium doped tellurite glass hosts primarily for 2 μm laser applications. Influence of the doping concentration and host composition on the strength of cross relaxation and luminescence quantum efficiency was investigated. We worked on thulium doped tellurite glasses with potassium and niobium oxide prepared at different Tm_2O_3 concentrations in order to investigate the influence of doping level on the quantum yields and cross relaxation mechanism: Tm_2O_3:(0.70)TeO_2-(0.15)K_2O-(0.15)Nb_2O_5 having Tm_2O_3 concentrations of 0.125, 0.25, 0.5, and 1.0 mol.%. By performing a Judd-Ofelt analysis of the absorption bands, we obtained average radiative lifetimes of 2.57±0.17 ms and 0.35±0.01 ms for the $^3H_4$ and $^3F_4$ levels, respectively. The highest quantum efficiency of 32 % was obtained for the sample doped with 0.125 mol. % Tm_2O_3 for the $^3H_4$ level. The average emission cross section of 6.01×10^{-21} cm^2 measured for the 1860-nm band reveals the potential of this host for the development of 2-μm lasers. Results also show that cross relaxation becomes

important as the ion concentration is increased, leading to the quenching of the 1460-nm band and relative enhancement of the 1860-nm emission.

In order to investigate the influence of the host composition on the strength of cross relaxation and quantum yields, we worked on tellurite glasses with different glass modifiers. Two tellurite based glass samples were prepared using niobium-oxide as a glass modifier: (x)Tm_2O_3 : (95)TeO_2 - (5-x) Nb_2O_5 (will be referred as TeNbTm-x) where x=1 and 0.25 mol.% and four samples were prepared using zinc-oxide as a glass modifier: (x)Tm_2O_3 : (80)TeO_2 – (20-x) ZnO (will be referred as TeZnTm-x), where x=1,0.5,0.25 and 0.125 mol.%. Judd-Ofelt analysis yields average radiative lifetime of 2.55±0.07 ms for the TeZnTm samples and 2.76±0.03 ms for the TeNbKTm samples for the $^3H_4$ level.

Average stimulated emission cross sections were obtained as $5.63x10^{-21}$ cm^2 for the TeNbTm sample and $6.33x10^{-21}$ cm^2 for TeZnTm sample for the 1860 nm emission band. These results compare well with values reported in the literature and for the TeZnTm sample we obtained higher stimulated emission cross sections (as high as $7.\ 36x10^{-21}$ cm^2) compared to values we previously reported for the 1860 nm emission band. Results suggest that, Tm^{3+} doped tellurite glasses possess a great potential for the development of the 2 μm laser sources for bulk as well as fiber applications. Hence, we expect that more work will be done in future to explore the spectroscopic and lasing characteristics of the tellurite glass family.

VITA

Adil Tolga Gorgulu was born in Izmir, Turkey on June 06, 1987. He received his BS degree both in Physics and Electrical & Electronics Engineering from Koç University University, Istanbul in 2009. At the same year he was admitted to the MS program in Materials Science and Engineering at Koç University. His studies were sponsored by TUBITAK BIDEB 2210 program. His research mainly focused on spectroscopic characterization, investigation and the development of novel laser sources and solid state lasers in the near and mid-IR. He will pursue his PhD degree in Physics at the University of Konstanz, Germany.

Publications:

A. T. Gorgulu, H. Cankaya, A. Kurt, A. Speghini, M. Bettinelli, and A. Sennaroglu, "Spectroscopic investigation of Tm3+:TeO2-K2O-Nb2O5 glasses at different doping levels for 2 μm laser applications," in Advances in Optical Materials, OSA Technical Digest (CD) (Optical Society of America, 2011), paper AIWB5.

Adil Tolga Gorgulu, Huseyin Cankaya, Adnan Kurt, Adolfo Speghini, Marco Bettinelli, and Alphan Sennaroglu, "Spectroscopic characterization of Tm^{3+}:TeO_2 -K_2O-Nb_2O_5 glasses for 2-μm lasing applications," Journal of Luminescence (in press).

BIBLIOGRAPHY

[1] T. J. Carrig, A. K. Hankla, G. J. Wagner, C. B. Rawle, and I. T. M. Kinnie, "Tunable infrared laser sources for DIAL," presented at SPIE Laser Radar Technology and Applications VII, 2002.

[2] T. Bilici, H. O. Tabakoglu, N. Topaloglu, H. Kalaycioglu, A. Kurt, A. Sennaroglu, and M. Gulsoy, "Modulated and continuous-wave operations of low-power thulium (Tm:YAP) laser in tissue welding," Journal of Biomedical Optics **15** (2010).

[3] J. S. Wang, E. Snitzer, E. M. Vogel, and J. G. H. Sigel, "1.47, 1.88, and 2.8 μm emission of Tm3+ and Tm3+-Ho3+ -codoped tellurite glasses," Journal of Luminescence **60-61**, 145-149 (1994).

[4] F. J. McAleavey, James O'Gorman, J. F. Donegan, B. D. MacCraith, J. Hegarty, and G. Maz´e, "Narrow Linewidth, Tunable Tm –Doped Fluoride Fiber Laser for Optical-Based Hydrocarbon Gas Sensing," IEEE JOURNAL OF SELECTED TOPICS IN QUANTUM ELECTRONICS **3**, 1103-1111 (1997).

[5] Y. H. Tsanga, D. J. Colemana, and T. A. King, "High power 1.9 μm Tm3+-silica fibre laser pumped at 1.09 μm by a Yb3+-silica fibre laser " Optics Communications **231**, 357-364 (2004).

[6] J. F. Wu, Z. D. Yao, J. Zong, and S. B. Jiang, "Highly efficient high-power thulium-doped germanate glass fiber laser," Optics Letters **32**, 638-640 (2007).

[7] J. S. Wang, E. M. Vogel, and E. Snitzer, "Tellurite glass: a new candidate for fiber devices," Optical Materials **3**, 187-203 (1994).

[8] M. Yamane and Y. Asahara, *Glasses for Photonics* (Cambridge University Press, 2000).

[9] H. Kalaycioglu, H. Cankaya, M. N. Cizmeciyan, A. Sennaroglu, and G. Ozen, "Spectroscopic investigation of Tm3+: TeO2-WO3 glass," Journal of Luminescence **128**, 1501-1506 (2008).

[10] X. L. Zou and H. Toratani, "Spectroscopic properties and energy transfers in Tm3+ singly- and Tm3+/Ho3+ doubly-doped glasses," Journal of Non-Crystalline Solids **195**, 113-124 (1996).

[11] O. V. Mazurin, M. V. Streltsina, and T. P. S.-. Shvaikovskaya, *Handbook of Glass Data: Single-Component and Binary Non-Silicate Oxide Glasses* (Elsevier, 1991).

[12] J. Azkargorta, I. Iparraguirre, R. Balda, and J. Fernández, "On the origin of bichromatic laser emission in Nd3+-doped fluoride glasses " J. Non-Cryst. Solids **16**, 11894-11906 (2008).

[13] N. Lei, B. Xu, and Z. H. Jiang, "Ti:sapphire laser pumped Nd:tellurite glass laser " Opt. Commun. **127**, 263-265 (1996).

[14] A. Mori, T. Sakamoto, K. Kobayashi, K. Shikano, Kiyoshi Oikawa, K. Hoshino, T. Kanamori, Y. Ohishi, and M. Shimizu, "1.58um Broad-Band Erbium-Doped Tellurite Fiber Amplifier," JOURNAL OF LIGHTWAVE TECHNOLOGY **20** (2002).

[15] J. S. Wang, D. P. Machewirth, F. Wu, E. Snitzer, and E. M. Vogel, "Neodymium-doped tellurite single-mode fiber laser," Opt. Lett. **19**, 1448-1449 (1994).

[16] K. Li, G. Zhang, and L. Hu, "Watt-level 2μm laser output in Tm3+-doped tungsten tellurite glass double-cladding fiber," Opt. Lett. **35**, 4136-4138 (2010).

[17] B. Richards, Y. Tsang, D. Binks, J. Lousteau, and A. Jha, "2 μm Tm3+/Yb3+-doped tellurite fibre laser " presented at Optical, Optoelectronic and Photonic Materials and Applications, London, UK 2007.

[18] Y. Tsang, B. Richards, D. Binks, J. Lousteau, and A. Jha, "Tm3+/Ho3+ codoped tellurite fiber laser," Opt. Lett. **32**, 1282-1284 (2008).

[19] B. Richards, S. Shen, and A. Jha, "A Infrared emission and energy transfer in Tm3+, Tm3+-Ho3+ and Tm3+-Yb3+-doped tellurite fibre," Optics Express **15**, 6546-6551 (2007).

[20] F. Fusari, A. A. Lagatsky, B. Richards, A. Jha, W. Sibbett, and C. T. A. Brown, "Spectroscopic and lasing performance of Tm3+-doped bulk TZN and TZNG tellurite glasses operating around 1.9 μm," Optics Express **16** (2008).

[21] F. Fusari, A. A. Lagatsky, G. Jose, S.Calvez, A. Jha, M. D. Dawson, W. Sibbett, and C. T. A. Brown, "Femtosecond mode-locked Tm3+ and Tm3+-Ho3+ doped 2 μm bulk glass lasers," Optics Express **18** (2010).

[22] A. A. Kaminskii, *Laser Crystals* (Springer, 1990).

[23] D. E. McCumber, "Einstein relations connecting broadband emission and absorption spectra," Physical Review B **136**, 954 - 957 (1964).

[24] D. J. Newman, "Theory of Lanthanide Crystal Fields," Adv. Phys. 20, 197-256 (1971).

[25] G. Racah, "Theory of Complex Spectra " Phys. Rev. 76 1352 (1949).

[26] C. J. Ballhausen, *Introduction to Ligand Field Theory* (McGraw-Hill, 1963).

[27] J. S. Griffith, *The Theory of Transition-Metal Ions* (Cambridge University Press, 1961).

[28] B. R. Judd, "Optical Absorption Intensities of Rare-Earth Ions," Physical Review 127, 750-761 (1962).

[29] G. S. Ofelt, "Intensities of crystal spectra of rare-earth ions," The Journal of Chemical Physics 37, 511 (1962).

[30] B. G. Wybourne, *Spectroscopic Properties of Rare Earths* (Wiley, 1965).

[31] L. J. F. Broer, C. J. Gorter, and J. Hoogschagen, "On the intensities and the multipole character in the spectra of the rare earth ions.," Physica 11, 231-250 (1945).

[32] J. J. Sakurai, *Modern Quantum Mechanics* (Addison Wesley, 1994).

[33] V. D. Rodriguez, V. Lavin, U. R. Rodriguez-Mendoza, and I. R. Martin, "Spectroscopy of rare earth ions in fluoride glasses for laser applications," Optical Materials **13**, 1-7 (1999).

[34] H. Gebavi, D. Milanese, R. Balda, S. Chaussedent, M. Ferrari, J. Fernandez, and M. Ferraris, "Spectroscopy and optical characterization of thulium doped TZN glasses," J. Phys. D: Appl. Phys. **43** (2010).

[35] A. Sennaroglu, I. Kabalci, A. Kurt, U. Demirbas, and G. Ozen, "Spectroscopic properties of Tm3+:TeO2-PbF2 glasses," Journal of Luminescence **116**, 79-86 (2006).

[36] P. F. Moulton, "Spectroscopic and Laser Characteristics of Ti-Al2O3," Journal of the Optical Society of America B-Optical Physics **3**, 125-133 (1986).

[37] V. Sudesh and E. M. Goldys, "Spectroscopic properties of thulium-doped crystalline materials including a novel host, La2Be2O5: a comparative study," Journal of the Optical Society of America B-Optical Physics 1068-1076 (2000).

[38] A. Sennaroglu, A. Kurt, and G. Özen, "Effect of cross relaxation on the 1470 and 1800 nm emissions in Tm3+:TeO2-CdCl2 glass," Journal of Physics: Condensed Matter **16**, 2471-2478 (2004).

[39] F. Fusari, S. Vetter, A. A. Lagatsky, B. Richards, S. Calvez, A. Jha, M. D. Dawson, W. Sibbett, and C. T. A. Brown, "Tunable laser operation of a Tm3+-doped tellurite glass laser near 2 μm pumped by a 1211 nm semiconductor disk laser," Optical Materials **32**, 1007-1010 (2010).

[40] Y. Z. Fang, M. L. Jin, L. Wen, S. G. Li, and L. L. Hu, "Er 3+ and Yb 3+ Codoped Phosphate Laser Glass for High Power Flashlamp Pumping " Chin. Phys. Lett. **24**, 1283-1286 (2007).

[41] D. O'Donnell, C. A. Miller, D. Furniss, V. K. Tikhomirov, and A. B. Seddon, "Fluorotellurite glasses with improved mid-infrared transmission " Journal of Non-Crystalline Solids **331**, 48-57 (2003).

[42] M. D. O'Donnell, K. Richardson, R. Stolen, A. B. Seddon, D. Furniss, V. K. Tikhomirov, C. Rivero, M. Ramme, R. Stegeman, G. Stegeman, M. Couzi, and T. Cardinal, "Tellurite and Fluorotellurite Glasses for Fiberoptic Raman Amplifiers: Glass Characterization, Optical Properties, Raman Gain, Preliminary Fiberization, and Fiber Characterization," Journal of the American Ceramic Society **90**, 1448-1457 (2007).